Babeş-Bolyai University, Faculty of Environmental Science and Engineering, Cluj-Napoca

LUMINESCENCE CHRONOLOGICAL STUDIES ON EUROPEAN AND NORTH AMERICAN LOESS-PALEOSOL SEQUENCES RECORDING LATE PLEISTOCENE-HOLOCENE CLIMATE CHANGES

Doctoral Thesis Summary

Viorica Tecșa

PhD Promoter: Prof. Dr. Alida Gabor (Timar)

Cluj-Napoca 2020

The luminescence dating investigations discussed in the present thesis were carried out at the Environmental Radioactivity and Nuclear Dating Centre, Interdisciplinary Research Institute on Bio-Nano-Science, Babeş-Bolyai University in Cluj-Napoca, Romania.

The magnetic susceptibility, grain size, and geochemical analysis presented in this thesis were carried out at the Bayreuth University, Germany and at the University of Wisconsin-Madison, USA.

Viorica Tecșa benefited from financial support from:

- The Romanian National Authority for Scientific Research, PN-III-P3-3.6-H2020-2016-0015 contract number 7/2016.
- European Research Council (ERC) under the European Union's Horizon 2020 research and innovation programme ERC-2014-StG 639904–RELOS.
- EEA-RO-NO-2018-0126 contract nr. 3/2019

Contents

Keywords: luminescence dating; fine quartz; coarse quartz; polymineral fine fraction; multi-proxy analysis; European loess-paleosol sequences; North American loess-paleosol sequences; Late Pleistocene; Holocene; past climate changes.

1. Introduction

1.1. Introduction

The Quaternary represents the most recent period of the geological record and is divided in two epochs: the Pleistocene and the Holocene. The Quaternary period spans the last ~ 2.6 Ma and is characteristic by cycling alternations of distinct glacial and interglacial environmental changes. The last interglacial-glacial cycle has been punctuated by two types of abrupt climate changes: abrupt warming and subsequent cooling in Greenland associated with Dansgaard-Oeschger (D-O) events (Dansgaard et al., 1984), and cold phases associated with Heinrich events (Heinrich, 1988) in the North Atlantic. The late Pleistocene was also punctuated by other abrupt climate events such as the Bølling-Allerød (B-O, ~14.7 to 12.9 ka) warm and the Younger Dryas (YD, ~12.9 to 11.7 ka) cold events (Alley and Clark, 1999). While the abrupt climate changes during the last glaciations are well documented in marine sediments (e.g., Bond et al., 1993; Schulz et al., 1998) and in Greenland ice cores (e.g., Dansgaard et al., 1993; Grootes et al., 1993), their manifestation elsewhere is less well constrained.

Loess-paleosol sequences (LPS) represent one of the most valuable terrestrial archives as they provide a high-resolution record of glacial-interglacial cycles of the Quaternary. In the most regions, loess was deposited during glacial periods whereas paleosols formed during warm-wet climate, specific to interglacial periods. However, previous studies indicated that there are some exceptions to the generalization of loess deposition occurring only in glacial periods (e.g. Roberts et al., 2001; Muhs et al., 2004; Miao et al., 2005; 2007a). Due to environmental differences between loess records from different continents, it is essential to establish proper chronologies of loess deposits. Previous studies demonstrated successful correlations between the main loess stratigraphic models and their equivalent marine isotope stage (MIS) (e.g., Lisiecki and Raymo, 2005). However, direct correlations of loess record with abrupt climate changes are still under debate and the main problem is represented by the inadequate age control (e.g. Rousseau et al., 2002, 2007; Antoine et al., 2009, 2013). In order to get a complete overview of the temporal and spatial diversity of the continental environmental change on a hemispheric scale, a high-resolution dating has to be included in the further studies on loess-paleosol sequences. Loess can be dated directly using methods, such as luminescence dating, a powerful technique for dating late Quaternary deposits.

Luminescence dating technique is a chronological method, which is typically applied to mineral grains of quartz and feldspar. These minerals can be stimulated in the laboratory with heat (thermoluminescence – TL) or with light (optically stimulated luminescence - OSL) and this gives rise to the emission of a light signal which is measured. This signal arises from exposure of the mineral grains to ionizing radiation (mainly decay of thorium, uranium, potassium and cosmic radiation) in the natural environment. The luminescence signal observed builds up steadily over time following deposition of the sediment grains. The mechanism of resetting the luminescence signal is represented by the typically exposure to sunlight during transport, in case of sedimentary grains. Thus, OSL dating can provide an estimate of the time since grains of quartz or feldspar were last exposed to sunlight (Aitken, 1998; Huntley et al., 1985). The burial age is estimated by dividing the equivalent dose (De, a measure of the radiation energy absorbed by a grain during the period of burial) by the environmental dose rate (the rate of supply of ionising radiation to the grain over the same period). The single-aliquot regenerative dose (SAR) protocol (Murray and Wintle, 2000; 2003; Wintle and Murray, 2006) represents the most commonly used method for the determination of the equivalent dose. The dose rate is calculated in this work based on the specific activities of natural isotopes from ^{238}U, ^{235}U, ^{232}Th series and ^{40}K determined by high-resolution gamma spectrometry.

In most of the OSL studies, the overall chronology has been established using a single grain size fraction, either the most representative or most abundant in the targeted deposit. Are there substantial differences in the age of quartz grains obtained on different granulometric fractions? Previous studies on loess sites from Europe and China reported unexpected age discrepancies between fine sand quartz fractions (grains larger than 63 microns) and silt-sized (4-11µm), although these differences are generally occurring for ages beyond 40-50 ka (Timar-Gabor et al., 2011, 2015; 2017; Constantin et al., 2014, 2015). There are two important reasons to carry out investigations on different grain sizes of quartz (e.g. 4-11 µm, 63-90 µm, 90-125 µm). First, if ages obtained on different grain sizes are in agreement, this is an argument for their accuracy. Secondly, a set of different ages (obtained for each sample) that are concordant allows for calculation of a weighted average age (Aitken, 1985 Appendix B) that better reflects the age of deposition and for which the random error is reduced. Further studies are required in order to test whether the luminescence ages of different particle size classes are in agreement in loess-paleosol sequences from different continents.

The results presented in this thesis are part of a research project financed by the European Research Council (ERC) (INTERTRAP- Integrated dating approach for terrestrial records of past climate using trapped charge methods, StG 678106, HORIZON 2020). This thesis makes a valuable contribution to the INTERTRAP project and provides the opportunity to test whether a robust luminescence chronology coupled with multi-proxy analysis (i.e. magnetic susceptibility, geochemistry, and grain size data) obtained on European and North American loess-paleosol sequences can provide a regionally coherent of the Late Pleistocene-Holocene climate changes.

1.2. Outline of the thesis

This thesis is comprised of 4 main chapters. Chapters 3 and 5 rely on articles I have authored (Tecsa et al., 2020a and b) and chapter 4 contains the results published in the article I have co-authored (Veres et al., 2018). **Chapter 1** presents the introduction part of this thesis. **Chapter 2** is based on the study of literature and provides the basics necessary to understand the studies presented in this thesis. **Chapter 3** presents a detailed optically stimulated luminescence dating coupled with results of a multi-proxy sedimentological and geochemical investigation of Kurortne loess-paleosol section from southwestern Ukraine. The aim of this study is to clarify local chronostratigraphic correlations, establish more secure reconstructions of Late Pleistocene environmental changes in the northern Black Sea area, and to test the correspondence with the Danube loess chronostratigraphic framework. **Chapter 4** provides a robust luminescence chronology for Stayky (Ukraine) based on optically stimulated luminescence dating on quartz (4-11 µm, 63-90 µm) and post infrared-infrared stimulated luminescence (pIR-IRSL) on polymineral fine grains. The aim of this study is to clarify several previously un-resolved chronostratigraphic issues for Stayky sequence. **Chapter 5** presents a detailed optically stimulated luminescence chronology as well as multi-proxy analysis obtained for the first time on the Enders and Kuma sections, located in southwestern Nebraska, central Great Plains. The aim of this study is twofold. Firstly, providing the first opportunity to investigate whether the luminescence ages of three different particle size classes are in agreement in important North American LPSs. Secondly, we wanted to test if LPSs in the central Great Plains can provide a regionally coherent record of the Pleistocene-Holocene transition and Holocene climatic change. At the end of the thesis conclusions are being summarised.

2. Luminescence dating of loess-paleosol sequences

2.1. Basic concepts of luminescence dating

2.1.1. Principles of optically stimulated luminescence dating

The luminescence signals observed arise from exposure of the sediment grains to ionizing radiation (mainly from the decay of uranium, thorium, potassium and from cosmic radiation) in the natural environmental, and the signal builds up steadily over time following deposition of the sediment grains. After the mineral is eroded, it is transported, deposited and exposed to sunlight during this time, consequently releasing the previously acquired energy and the luminescence signal is reset to zero. Upon burial, the luminescence signal starts again to build up in time, and the larger radiation dose, the greater the OSL signal will be. The luminescence signal accumulated by the minerals from the last zeroing event (last exposure to sunlight) can be removed in the laboratory by exposing the mineral grains to light or heat.

The depositional age of a sediment is equal to the equivalent dose, De (Gy) of the sample divided by its annual dose rate (Gy/a). The annual dose rate is determined in this work by high-resolution gamma spectrometry and the most commonly used method for De determination is the single-aliquot regenerative-dose (SAR) protocol (Murray and Wintle, 2000, 2003).

2.1.2. Luminescence mechanism

Although the mechanism of luminescence production is complex and not yet fully understood, the main processes of causing luminescence in quartz can be described in terms of the energy level diagram (Aitken, 1998). This simplified model is referred to as the „one trap/one centre" model involving only one trap (T) and one recombination centre (L) configuration. However, the natural quartz crystals are complex systems in which more than one type of traps and recombination centers compete for charge. The luminescence process has three initial steps in charge transfer (ionization, storage, and eviction) that can be illustrated using a schematic energy band diagram.

2.1.3. The single-aliquot regenerative-dose technique (SAR)

The SAR protocol requires constructing an OSL dose-response curve by repeatedly preheating, dosing, and optically stimulating a sample (see **figure 2.1**).

Figure 2.1. The SAR protocol redrawn after Murray and Wintle (2003). L_x is the natural or regenerated signal and T_x is the test dose signal.

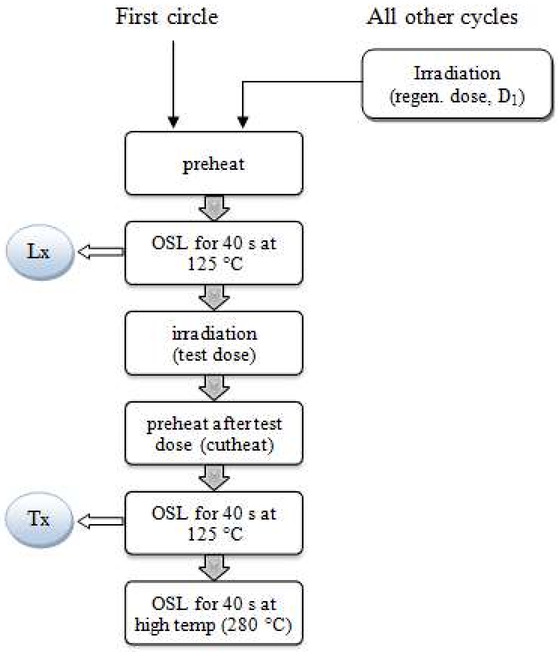

In order to evaluate the performance of the SAR procedure, recuperation, recycling and IR depletion tests are used as a criterion for acceptance or rejection of aliquots. In order to assess the influence of preheat temperature on equivalent dose estimates, a preheat test can be used by plotting the equivalent dose value as a function of preheat temperature. The ultimate test for evaluating the performance of SAR procedure is the dose recovery test, which is used to check if a known dose given in the laboratory can be accurately recovered in the SAR protocol.

2.1.4. Minerals and grain sizes used for dating

The most widely used minerals in luminescence dating are quartz and feldspars. The choice of quartz grain size used for dating depends on the dominant grain size present in the particular sedimentary unit and most dating studies have been based on the tradition of OSL using a single grain size fraction. Although it was assumed that different granulometric fractions should yield similar luminescence ages, previous luminescence studies on several Chinese loess sites (Timar-Gabor et al., 2017) as well as European loess sites (e.g. Timar-Gabor et al., 2011, 2015; Constantin et al., 2014, 2015) reported unexpected age discrepancies between silt sized (4-11µm) and fine sand quartz fractions (grains larger than 63 µm). More precisely, these differences are generally occurring for ages beyond 40-50 ka.

2.1.5. Sample preparation

Sample preparation is performed in the laboratory under low intensity red light, to avoid bleaching of the luminescence signal. The preparation protocol for extraction of quartz (Aitken, 1985) involves several steps including acid treatments, sieving, density separation, separation based on Stokes‘s law and centrifugation in distilled water.

2.1.6. Instrumentation

In order to determine the equivalent dose, the measurements were carried out using standard and automated Risø TL/OSL-DA-20 readers equipped with classic or automated detection and stimulation head (DASH) (Lapp et al., 2015).

The dose rate is calculated based on the specific activities of natural isotopes from ^{238}U, ^{235}U, ^{232}Th series and ^{40}K determined by high-resolution gamma spectrometry.

2.2. Loess as an archive recording past climate changes

Loess represents sediment that has been entrained, transported, and deposited by the wind, typically composed of quartz, feldspars, plagioclase, carbonates, micas, clay minerals, and heavy minerals (Pye, 1987). Loess has become one of the most important archives of Quaternary climate change in the last 150 years and it can be used to reconstruct synoptic-scale paleoclimatology over millennial timescales (Muhs, 2013). Loess deposits and intercalated paleosols (buried soils) provide one of the most complete terrestrial records of interglacial-glacial cycle. The advantage of loess compared to other Quaternary sediments (alluvium, colluvium or till) is that it can be dated directly using methods, such as luminescence geochronology (Aitken, 1998). The measurement of magnetic susceptibility and other mineral magnetic properties represent the most common method applied to loess-derived paleosols for paleoclimate studies (Verosub et al., 1993; Maher et al., 1994; Porter, 2001; Singer and Verosub, 2007).

2.3. Glacial-interglacial - scale loess correlations

Valid correlations for loess on regional or even continental scales are only possible at the level of first order units (i.e. MIS or glacial loess and interglacial pedocomplex units), although recent research has provided significant progress on inter-profile correlations and direct comparison of different palaeoclimatic records (Marković et al., 2018).

Studies of loess-paleosol sequences took a simple relative dating approach, counting the modern developed soil (Holocene) as equivalent to the last interglacial, and older soils are correlated with earlier interglacial episodes. Loess horizons are labeled L_i while the intercalated palaeosols S_i. Generally, loess was deposited during glacial periods, and soils formed during interglacial periods. However, there are some exceptions to the generalization of loess deposition occurring only in glacial periods.

Although the successful attempts at correlations between the main loess stratigraphic models and their equivalent MIS (e.g., Lisiecki and Raymo, 2005), application of event stratigraphy in loess research is still problematic. For instance, direct correlations of loess record with abrupt climate changes (e.g. Rousseau et al., 2002, 2007; Antoine et al., 2009, 2013) are still under debate and the main problem lies in inadequate age control.

2.4. Abrupt climate changes

High-resolution paleoclimatic records from sediment cores, ice, and other sources, present a number of abrupt climate changes that show up over surprisingly short time scales (i.e. a few decades or few years). According to the U.S. National Research Council, a definition of „an abrupt climate change" is any change that occurs when the climate system is forced to cross a threshold (National Research Council, 2001).

The last climate cycle (Marine Isotope Stages 4, 3 and 2; ~130-12 ka) was characterised by millennial-scale climate oscillations of irregular periodicity. There have been described two types of rapid climate changes: Dansgaard–Oeschger (D-O) cycles (Dansgaard et al.,1984) and cold phases associated with Heinrich events (Heinrich, 1988). The D-O cycles represent one of the best observed yet most intriguing examples of abrupt climate change and they are characterized by fast (decadal or shorter) transitions between full glacial conditions (Greenland Stadial, GS) and mild climate (Greenland Interstadial, GI) lasting many centuries (Svensson et al., 2006).

Other abrupt climate events occurred in the late Pleistocene are the Bølling-Allerød (B-O, ~14.7 to 12.9 ka) warm and the Younger Dryas (YD, ~12.9 to 11.7 ka) cold events (Alley and Clark, 1999).

2.5. Abrupt climate changes recorded in loess

Loess deposits, especially in Northern Hemisphere, have recorded past climate changes at millennial and sub-millennial timescales. Previous studies indicated the evidence of abrupt climate changes recorded in loess sequences from Europe (e.g. Rousseau et al. 2002; 2007, 2011; Sima et al. 2009; 2013; Antoine et al., 2009; 2013), Central Asia (e.g. Vanderberghe et al., 2006) and China (Porter and An, 1995; Sun et al., 2012). On the other hand, evidence for abrupt climate changes has rarely been reported in the North American loess records.

2.6. Luminescence dating studies of abrupt climate events in European loess

Rousseau et al. (2011) investigated an eastern European key loess section (Stayky) located in Ukraine using multy proxy analyses and infrared stimulated luminescence (IRSL) dating. Four ages have been reported ranging between 16-30 ka using polymineral fine grains (4-11 µm). The embryonic soils (ES) identified in Bug loess have been associated with the Greenland interstadials (GIS) 7 to 2, and the Vytachiv cambisol (IRSL age of 30.2±3.1 ka) with GIS 8 (Rousseau et al., 2011). The authors have also suggested that the first strong increase in grain-size index (prior to the IRSL age of 27.6±2.7 ka) corresponds to Heinrich event (H) 3 and its maximum increase (after 27.6±2.7 ka) was linked to H2. However, Kadereit and Wagner (2014) suggested that the correlation of the embryonic soils above the Vytachiv soil presumably does not start with GIS7 but probably after GIS5 and the lowermost incipient soils from Bug loess (ES8 to ES5/4b) probably developed during the final phase of MIS 3.

Sub-millennial timescale climate variations correlated with those in the North Atlantic area are also identified in the western European key loess section at Nussloch, Germany (Antoine et al., 2001, 2009). Rousseau et al. (2011) proposed a correlation between Nussloch and Stayky sequences based on the available dates and the stratigraphic similarities.

Dolní Věstonice (DV) loess section is located in the central part of the European loess belt and is well known for its high-resolution loess–palaeosol sequence of the last interglacial–glacial climatic cycle. This loess section is characterised by four pedosedimentary subsequences (I to IV). According to the OSL chronology, as well as to the palaeopedological and sedimentological investigations, the soil complex (subsequence I) of Dolní Věstonice loess section recorded all of the main climatic events expressed in the North GRIP record from Greenland Interstadials 25 to 19 (Fuchs et al., 2012; Antoine et., 2013).

3. Dating study of Kurortne (Ukraine): classical section recording only major climate shifts - based on Tecsa et al. (2020a)

3.1. Introduction

The aim of this study is to clarify local chronostratigraphic correlations, establish more secure reconstructions of Late Pleistocene environmental changes in the northern Black Sea area. Here we discuss Late Pleistocene environmental dynamics in southwestern Ukraine based on integrating optically stimulated luminescence dating of quartz of different grain sizes (4-11 µm, 63-90 µm and 90-125 µm), with high-resolution rock magnetic data, grain size and geochemical proxies for Kurortne loess-paleosol sequence (LPS). Through comparison with other records from the Danube-Black Sea loess fields we show that the investigated sequence extends over the Last Glacial Cycle (LGC), providing an important link to other regional LPS, and a key record for comparison of the Ukrainian Quaternary stratigraphy with the Danube loess model (Marković et al., 2015).

3.2. Study site

The Kurortne LPS (45°54' N, 30°16' E) is located near Kurortne village (Odessa region, Ukraine), at the Black Sea shore. The section comprises ca. 15 m of intercalated loess and paleosol units (Gozhik et al., 2000), and for this study we have investigated in detail the uppermost 4.5 m (**Fig. 3.1**). In order to augment the existing chronostratigraphic framework for Kurortne LPS, 12 samples were collected for optically stimulated luminescence (OSL) dating. For sedimentological and geochemical analyses samples were collected contiguously at 2 cm resolution down to 130 cm depth, whereas to the depth of 450 cm sampling was carried out at 4 cm resolution.

3.3. Methods and instrumentation

3.3.1. Sedimentological analyses

The sedimentological analyses were carried out at Bayreuth University from Germany.

The rock magnetic measurement protocol follows Zeeden et al. (2018) with the dried material filled into 6.4 cm^3 plastic boxes, compressed, and fixed with cotton wool to prevent movement of particles during analytical measurements. The magnetic susceptibility χ was measured at frequencies of 0.31 kHz (ie., χ_{lf}) and 3 kHz (ie., χ_{hf}) using a Magnon International

VSFM. The frequency dependent magnetic susceptibility was calculated as $\chi_{fd}=(\chi_{lf}-\chi_{hf})/\chi_{lf} * 100$ [%] (**Fig. 3.1**).

The particle size distribution was measured with a Laser Diffraction Particle Size Analyzer (Beckman Coulter LS 13 320), by calculating the percentage size frequency of 116 classes within a size range of 0.04–2000 µm with an error of 2% (expressed by the coefficient of variation, CV). The classic grain size distribution was determined by applying the Mie theory (Fluid RI: 1.33; Sample RI: 1.55; Imaginary RI: 0.1; Özer et al., 2010; ISO 13320, 2009; Schulte et al., 2016).

In order to assess the long-term geochemical variability at Kurortne, the concentration of selected elements was measured on the fine-grained fractions extracted by sieving out material <63 µm and drying it at 105 °C for 12 hours. All samples were measured twice with a SpectroXepos X-ray fluorescence (XRF) device. Subsequently, mean values were calculated from the two measurements following the instructions of Spectro (2007), and variability in selected major oxide data is discussed in **Figure 3.1**. The chemical index of alteration (CIA) was calculated according to Nesbitt and Young (1982): CIA = $[Al_2O_3 / (Al_2O_3+Na_2O + CaO^* + K_2O)] * 100$ (in molar proportions; CaO* refers to silicatic Ca).

3.3.2. Optically stimulated luminescence (OSL) dating

Twelve samples were collected for luminescence dating from Kurortne LPS in order to extract fine (4-11 µm) and coarse (63-90 µm and 90-125 µm) quartz. Luminescence measurements were carried out using two Risø TL/OSL-DA-20 readers equipped with classic or automated detection and stimulation heads (DASH) (Lapp et al., 2015), whereas luminescence signals were detected by EMI 9235QA and PDM 9107Q-AP-TTL-03 photomultiplier tubes (Thomsen, 2006). Luminescence characteristics of fine (4-11 µm) and coarse (63-90 µm and 90-125 µm) quartz grains were analysed using the single-aliquot regenerative dose (SAR) protocol (Murray and Wintle, 2000; 2003). The robustness of the SAR protocol was checked by the intrinsic performance tests (recycling and recuperation) (Murray and Wintle, 2003). The purity of the quartz grains extracted was evaluated on all aliquots measured using OSL IR depletion test (Duller, 2003).

High-resolution gamma spectrometry was applied for determining the radionuclide activity concentrations. The values for the total dose rates as well as the radionuclide concentrations for these samples are given in **Table 3.1**.

3.4. Results and Discussion

3.4.1. Sedimentological and geochemical data

The χ record of Kurortne LPS shows high values for paleosols and lower values in loess, varying between 28 10^{-8} m^3/kg (the Uday loess) to 94 10^{-8} m^3/kg (the Holocene soil) (**Fig. 3.1**). The χ_{fd} parallels the trend in χ_{lf} (**Fig. 3.1**), the two proxies being well correlated (R^2=0.648), but showing more variability in the Pryluky, Uday and Vytachiv units. χ_{fd} generally oscillates around 11% in the Kaydaky unit and the Holocene soil, reaching lower minima of 6-7% in the Vytachiv and Bug units (**Fig. 3.1**). A magnetic susceptibility threshold at Kurortne can be discerned at the end of the proper loess formation of the Bug unit. Thus, it is possible to place around 1 m depth the end of the pleniglacial loess formation and the onset of pedogenic processes that lead to the formation of the incipient soils of the Middle Prychornomorya subunit, and subsequently to the formation of the Holocene S0 soil.

Figure 3.1 shows the geochemical data denoting concurrent variability in all major oxides between paleosols and the loess units that is well reflected in the lithostratigraphy. The SiO_2 values ranges from 42.7% to 62.7% (average 52.3%), whereas Al_2O_3 varies between 7.8% and 12.7%, with an average of 10.4%. Other major oxides are present in smaller concentrations. CaO reaches values between 1.2% and 14.9% (average 7.5%) and it reflects well the lithostratigraphic changes, attaining highest values in both the Dnipro, Uday, and Bug loess units and the lower parts of Kaydaky and Vytachyv soils, and lowest values in the Holocene soil.

The main component of the grain size distribution is in the cSi (ie., 20-63 µm) fraction for the whole data set. The <2 µm fraction shows high values in the Kaydaky soil and at the transition from the Vytachiv soil to the Uday loess. The continuous increase in 2-20 µm fraction may reflect a long-term decrease in wind intensity. The >63 µm fraction has the smallest proportion in the Kaydaky soil, and the 20-63 µm fraction shows low values both in the Kaydaky and Vytachiv paleosols.

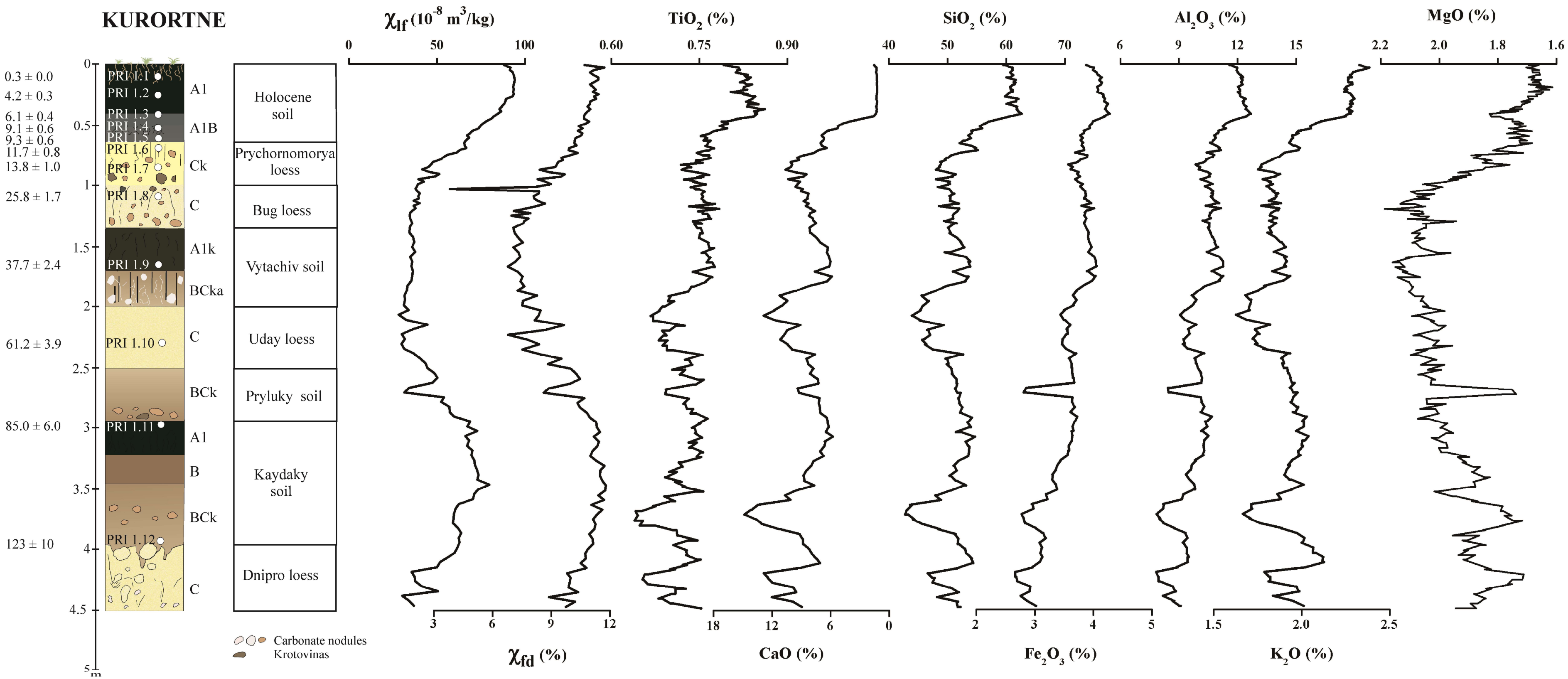

Figure 3.1. The lithostratigraphy and weighted average ages of the investigated uppermost 4.5 m at Kurortne loess-paleosol section, alongside the identified regional chronostratigraphic units of the Ukrainian Quaternary stratigraphic framework. The two oldest samples (PRI-1.11-1.12) provide ages only on 63-90 µm quartz extracts. The sedimentological data include the low-frequency magnetic susceptibility (χ_{lf}), frequency-dependent magnetic susceptibility (χ_{fd}) and the relative abundance (in %) of major oxides TiO_2, CaO, SiO_2, Fe_2O_3, Al_2O_3, K_2O, and MgO. Note the reversed horizontal axis for CaO and MgO. Krotovinas are marked by light-brown and brown patches, and carbonate concretions by beige patches. The location of OSL samples is also indicated.

3.4.2. Luminescence properties and equivalent doses

The equivalent doses (D_e) were obtained by projecting the sensitivity corrected natural OSL signal onto the dose response curve constructed for each luminescence sample.

The dependency of the equivalent doses on the preheat temperature was investigated for sample PRI-1.7. As shown in **Figure 3.2**, the preheat plateau indicates the thermal stability of the OSL signal and ensures that any thermal transfer is irrelevant. The recycling ratio and recuperation were satisfactory for all measured aliquots.

Figure 3.2. Equivalent dose dependence on preheat temperatures for fine (4-11 µm) and coarse (63-90 µm) quartz fractions from sample PRI 1.7. A 180°C cutheat (test dose preheat) was employed.

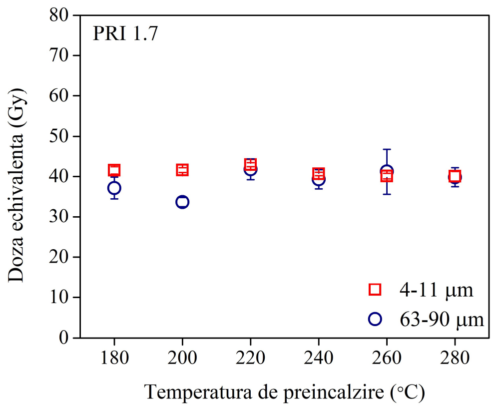

Dose recovery tests (Murray and Wintle, 2003) were conducted to investigate the reliability of the equivalent doses obtained by applying the SAR protocol on fine (4-11 µm) and coarse (63-90 µm) quartz grains from samples PRI-1.2, 1.4, 1.6, 1.8 and PRI-1.10. As seen in **Figure 3.3**, very good recovery to given dose ratios were obtained, except for PRI-1.2 (4-11 µm quartz fraction) showing 14% underestimation.

Figure 3.3. Dose recovery test results for fine (4-11 µm) and coarse (63-90 µm) quartz fractions from five samples. The given irradiation doses were chosen to match the equivalent dose of each sample. The solid line indicates the ideal 1:1 dose recovery ratio while the dash lines bracket a 10% variation from unity.

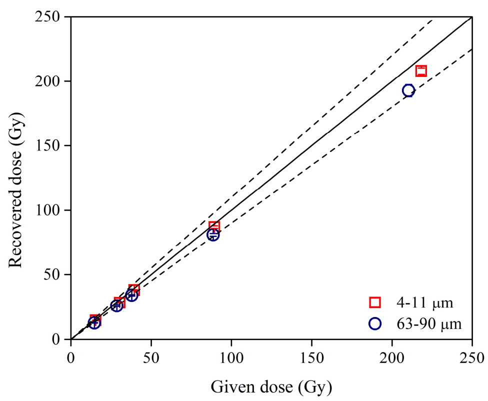

Dose response for very high doses was investigated using three aliquots from sample PRI-1.12 (Dnipro loess), and sensitivity corrected growth curves extending up to 5000 Gy were constructed on fine (4-11 μm) and coarse (63-90 and 90-125 μm) quartz grains **(Fig. 3.4)**. The growth curve was best fitted by a sum of two saturating exponential function such as in the following equation:

$$I(D) = I_0 + A(1 - \exp(-D/D_{01})) + B(1 - \exp(-D/D_{02}))$$

where, I is the intensity of the signal for a given dose D, I_0 is the intercept, A and B are the saturation intensities of the two exponential components and D_{01}, D_{02} are the dose levels characteristic of the dose–response curve of each exponential function.

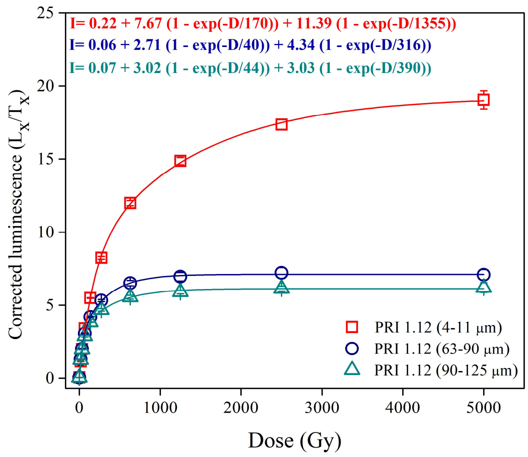

Figure 3.4. Comparison between extended dose-response curves constructed for sample PRI 1.12 using fine 4-11 μm quartz grains, coarse 63-90 μm and 90-125 μm quartz grains. A test dose of 17 Gy was used throughout the measurements. Data presented is the average obtained on 3 aliquots.

From data presented in **Figure 3.4** it can be observed that the fine quartz fraction (4-11 μm) saturates at significantly higher doses than coarse (63-90 μm and 90-125 μm) fractions. From doses higher than about 100 Gy a significant difference in the response between fine and coarse-grained quartz was observed. Different saturation characteristics of fine and coarse quartz grains have been reported previously in loess samples from southestern Europe and the Chinese Loess Plateau (CPL) (Timar-Gabor et al., 2012; 2015; 2017).

3.4.3. OSL ages and validity of regional correlations based on luminescence data

Table 3.1 presents a summary of the age results, with uncertainties on the individual ages obtained based on the error assessment system by Aitken and Alldred (1972) and Aitken (1976).

For samples PRI-1.12 and 1.11 collected in the BCk horizon of the Kaydaky paleosol and at the Pryluky-Kaydaky soil boundary, coarse (63-90 µm) quartz ages 123±10 ka and of 85±6 ka, respectively, were obtained. These ages would confirm the correlation of Kaydaky and Pryluky paleosol units with MIS 5 (Rousseau et al., 2001; Gerasimenko, 2004, 2006; Buggle et al., 2009; Veres et al., 2018) (**Fig. 3.1**). The OSL ages obtained for the transition between the Pryluky and Kaydaky units broadly agree with the OSL ages of 70.1±4.0 ka and 93.6±5.6 ka obtained on 90-125 µm quartz grains, reported by Gozhik et al. (2014) for Pryluky unit in the Maxymivka section, situated in the Dnieper Plain. The ages reported for the Pryluky-Kaydaky paleosols at Kurortne are in a very good agreement with results obtained on several LPS at the Black Sea in Romania, where the paleosol (ie., S1) underlying the uppermost loss (L1) unit was correlated to MIS 5 (Timar et al., 2010; Timar-Gabor et al., 2011; Constantin et al., 2014).

The weighted average age of 61.2±3.9 ka yielded for the Uday loess sample attributes this unit to the lower pleniglacial (MIS 4; **Fig. 3.1**) and agrees within errors with the TL-age of 65.9±10 ka, obtained on 80-100 µm quartz grains reported by Gozhik et al. (2014).

Sample PRI-1.9, collected from A1k horizon of Vytachiv unit at Kurortne, provided a weighted average age of 37.7±2.4 ka and enables the correlation of this unit with MIS 3. The available ^{14}C and luminescence data on the Vytachiv paleosol unit in the Middle Dnieper area (Gerasimenko, 2004; Bokhorst et al., 2011; Rousseau et al., 2011; Kadereit and Wagner, 2014) further enable the broad correlation of this unit with MIS 3. This is further supported by radiometric data discussed in Gozhik et al. (2014) that suggested the better-resolved Vytachiv unit at the Maxymivka sequence comprises most of MIS 3. At Stayky, also located in Middle Dnieper area, Veres et al. (2018) also attributed the truncated Vytachiv paleosol unit to within middle to late MIS 3.

The weighted average age 25.8±1.7 ka for the Bug loess unit allows its correlation with the upper pleniglacial (MIS 2) (**Fig. 3.1**). This age is in agreement with OSL ages of 25.8±1.3 ka and 21.1±0.9 ka obtained on 90-125 µm quartz grains from the two samples collected from the lower and upper part of the Bug unit elsewhere (Gozhik et al., 2014).

Table 3.1. Summary of the luminescence and dosimetry data. Weighted OSL ages are calculated according to Aitken (1985). The uncertainties associated with the luminescence and dosimetry data are random; the uncertainties mentioned with the optical ages are the overall uncertainties. All uncertainties represent 1σ. The ages were determined considering the "as found" water content, with a relative error of 25%; n denotes the number of accepted aliquots; beta attenuation and etching factor used for 63-90 μm and 90-125 μm fractions are 0.94±0.050 and 0.92±0.050, respectively; adopted alpha efficiency factor was 0.04±0.02. The total dose rate consists of the contribution from the alpha, beta and gamma radiations as well as the contribution from the cosmic radiation.

Sample code	Grain size(μm)	Water content (%)	De (Gy)	U-Ra (Bq/kg)	Th (Bq/kg)	K (Bq/kg)	Total random error (%)	Total systematic error (%)	Total dose rate(Gy/ka)	Age (ka)	Weighted ages (ka)
PRI 1.1	4-11	4.4	3.5 ± 0.1 (n=11)	42.8 ± 1.3	40.6 ± 1.2	508 ± 15	3.2	7.9	4.00 ± 0.06	0.9 ± 0.1	0.3 ± 0.0
	63-90		1.1 ± 0.1 (n=10)				9.2	5.5	3.36 ± 0.05	0.3 ± 0.0	
	90-125		0.8 ± 0.1 (n=10)				12.6	5.4	3.32 ± 0.05	0.2 ± 0.0	
PRI 1.2	4-11	6.2	15.4 ± 0.1 (n=11)	41.3 ± 1.5	39.4 ± 1.5	507 ± 14	1.8	7.9	3.83 ± 0.06	4.0 ± 0.3	4.2 ± 0.3
	63-90		14.7 ± 1.4 (n=10)				9.7	5.6	3.22 ± 0.05	4.6 ± 0.5	
	90-125		13.8 ± 1.1 (n=12)				8.1	5.6	3.18 ± 0.05	4.3 ± 0.4	
PRI 1.3	4-11	2.8	24.0 ± 0.7 (n=11)	38.6 ± 0.1	41.6 ± 1.1	485 ± 16	3.3	7.9	3.87 ± 0.06	6.2 ± 0.5	6.1 ± 0.4
	63-90		24.1 ± 2.3 (n=10)				9.7	5.4	3.24 ± 0.05	7.4 ± 0.8	
	90-125		17.2 ± 1.4 (n=12)				8.3	5.4	3.20 ± 0.05	5.4 ± 0.5	
PRI 1.4	4-11	2.2	30.4 ± 0.4 (n=10)	37.0 ± 0.9	33.4 ± 0.8	447 ± 13	2.0	7.8	3.52 ± 0.05	8.6 ± 0.7	9.1 ± 0.6
	63-90		28.7 ± 2.0 (n=10)				7.1	5.4	2.96 ± 0.05	9.7 ± 0.9	
	90-125		26.7 ± 1.4 (n=12)				5.5	5.4	2.92 ± 0.05	9.1 ± 0.7	
PRI 1.5	4-11	6.7	32.6 ± 0.7 (n=11)	37.3 ± 0.3	35.2 ± 0.3	453 ± 13	2.5	8.0	3.41 ± 0.04	9.6 ± 0.8	9.3 ± 0.6
	63-90		26.6 ± 1.5 (n=11)				5.8	5.6	2.87 ± 0.04	9.3 ± 0.8	
	90-125		26.2 ± 1.0 (n=12)				4.1	5.6	2.83 ± 0.04	9.2 ± 0.6	
PRI 1.6	4-11	6.5	39.5 ± 0.4 (n=12)	38.2 ± 1.4	35.5 ± 1.3	496 ± 16	2.1	7.8	3.58 ± 0.07	11.0 ± 0.9	11.7 ± 0.8
	63-90		37.9 ± 1.6 (n=10)				4.6	5.7	3.02 ± 0.06	12.5 ± 0.9	
	90-125		34.8 ± 2.6 (n=12)				7.7	5.6	2.99 ± 0.06	11.7 ± 1.1	
PRI 1.7	4-11	8.5	42.9 ± 0.5 (n=10)	36.1 ± 1.0	33.4 ± 1.3	448 ± 12	2.0	8.1	3.25 ± 0.05	13.2 ± 1.1	13.8 ± 1.0
	63-90		41.8 ± 2.6 (n=11)				6.4	5.8	2.74 ± 0.04	15.3 ± 1.3	
	90-125		36.1 ± 2.5 (n=10)				7.1	5.8	2.70 ± 0.04	13.4 ± 1.2	
PRI 1.8	4-11	7.7	89.4 ± 1.1 (n=10)	38.0 ± 1.1	39.4 ± 0.5	447 ± 13	1.8	8.3	3.45 ± 0.05	25.9 ± 2.2	25.8 ± 1.7
	63-90		88.7 ± 4.0 (n=10)				4.7	5.7	2.88 ± 0.04	30.8 ± 2.3	
	90-125		62.8 ± 4.1 (n=12)				6.7	5.7	2.85 ± 0.04	22.0 ± 1.9	
PRI 1.9	4-11	4.2	123 ± 1 (n=10)	33.1 ± 1.5	36.5 ± 1.0	458 ± 13	1.9	7.8	3.41 ± 0.06	36.2 ± 2.9	37.7 ± 2.4
	63-90		111 ± 5 (n=10)				4.9	5.5	2.87 ± 0.05	38.7 ± 2.8	
	90-125		108 ± 4 (n=12)				3.8	5.5	2.84 ± 0.05	38.0 ± 2.5	
PRI 1.10	4-11	1.5	218 ± 1 (n=11)	36.5 ± 0.4	40.0 ± 0.7	458 ± 14	1.5	8.0	3.68 ± 0.05	59.3 ± 4.8	61.2 ± 3.9
	63-90		210 ± 10 (n=14)				5.2	5.4	3.07 ± 0.05	68.5 ± 5.1	
	90-125		177 ± 6 (n=22)				3.8	5.4	3.03 ± 0.05	58.3 ± 3.8	
PRI 1.11	4-11	6.7	248 ± 1 (n=11)	32.8 ± 1.3	39.9 ± 1.0	472 ± 15	1.8	8.0	3.41 ± 0.06	72.8 ± 6.0	-
	63-90		243 ± 9 (n=10)				4.2	5.7	2.86 ± 0.05	85.0 ± 6.0	
	90-125		235 ± 13 (n=12)				5.8	5.7	2.83 ± 0.05	83.0 ± 6.7	
PRI 1.12	4-11	9.7	283 ± 3 (n=10)	28.7 ± 0.2	33.4 ± 1.5	461 ± 15	2.1	7.9	3.01 ± 0.06	94.2 ± 7.7	-
	63-90		313 ± 15 (n=10)				5.2	6.0	2.55 ± 0.05	123 ± 10	
	90-125		280 ± 11 (n=10)				4.5	6.0	2.52 ± 0.05	111 ± 8	

The dates obtained on the Bug loess at Stayky in the Middle Dniper area (Rousseau et al., 2011; Veres et al., 2018) also are in agreement with a MIS 2 age.

For samples taken from the Holocene soil and over the transition to the Bug loess, weighted average ages ranging from 0.3 ka to 13.8 ka have been obtained (**Fig. 3.1**). The transition from the Pleistocene loess to the Holocene soil was identified on the basis of magnetic susceptibility threshould at around 1 m depth, thus prior to 13.8 ka. Thus, the OSL ages show that the onset of magnetic susceptibility enhancement at Kurortne precedes the accepted stratigraphic Pleistocene-Holocene boundary dated at 11.7 ka in ice core records (Rasmussen et al., 2014). Similar results have been reported by Constantin et al. (2019) for Roxolany site in Ukraine, as well as in loess-paleosol sites across Romania and Serbia.

3.5. Regional correlations based on lithological, pedological and environmental magnetic data

The correlation of the Ukrainian stratigraphic units Uday loess, Vytachiv paleosol complex and Bug loess to MIS 4, MIS 3 and MIS 2, respectively, was reported in the previous investigations based on pedostratigraphical, palynological and magnetic susceptibility data (Gozhik et al., 2000, 2001, 2014; Rousseau et al., 2001, 2011; Gerasimenko, 2004, 2011; Buggle et al., 2008, 2009; Bokhorst et al., 2011; Veres et al., 2018). Two opposite views exist however on the correlation of Pryluky, Tyasmyn, Kaydaky and Dnipro units with MIS stages, as well as on the overall stratigraphy of loess plateau sections in the Black Sea region. Both our field and analytical data would confirm that the chernozem paleosol (Kaydaky unit; ie., S1SS2) identified between 2.90-4.1 m depth (**Figs 3.1**) is a well developed paleosol, which, judging from its thickness and the depth position of the carbonate horizon, belongs to the same genetic type of chernozems as the modern S0 chernozem (Krupsky and Polupan, 1979). According to the χ data (**Figs 3.1**), the Kaydaky unit is the only paleosol which can be compared to the Holocene S0 and, thus, to an interglacial soil. At Kurortne, the Pryluky unit (ie., S1SS1) is partly truncated (only the BCk horizon identifiable; **Fig. 3.1**) but, in general, in this area it is represented by chernozems of subtype 'southern' or by kastanozems (Sirenko and Turlo, 1986). The χ values are lower in the Pryluky unit than in the interglacial Kaydaky unit (**Figs 3.1**).

The Uday loess unit (ie., L1LL2) likely corresponds to the climate cooling of the early pleniglacial as reflected in the sharp decrease in χ (**Fig. 3.1**). The fact that the Uday loess unit is more clayey and less enriched in coarse silt than Bug or Dniper loesses led the aforenamed Ukrainian authors to suggest less energetic wind speed at the beginning of the early pleniglacial. The upper part of the Vytachiv unit (i.e., L1SS1) as preserved at Kurortne can be related to the middle Vytachiv paleosol (it shall be noted that in most complete sections of the Vytachiv unit, the middle soil of MIS 3 (Vytachiv) pedocomplex is dated between 36-38 ka BP). χ values are somewhat higher in the lower Vytachiv paleosol than in the middle one (Buggle et al., 2008, 2009; Bokhorst et al., 2011), as observed also at Kurortne (**Fig. 3.1**) and probably characteristic for the southeastern Europe, including the Black Sea region (Obreht et al., 2017).

The thickness of the Bug loess (ie., L1LL1) at Kurortne is much less compare to profiles up to 8-12 m reported in northern Ukraine (Gerasimenko, 2006; Rousseau et al., 2011).

The identified succession of climatic events at Kurortne can be correlated with other similar LGC loess records in southeastern Europe (e.g. Mircea Voda, Costinesti¸ Koriten and Semlac sections) (Constantin et al., 2014; Necula et al., 2013, 2015; Timar-Gabor et al., 2011; Jordanova and Petersen, 1999; Zeeden et al., 2016), and with the astronomically tuned χ record from the Titel/Stari Slankamen composite record from Serbia on its own age scale (Basarin et al., 2014). All records show similar (climato) stratigraphic characteristics that, however, are temporarily better resolved in the thicker sequences (ie., Mircea Voda, Koriten, Titel). Nevertheless, also the condensed sections with thicknesses of less than 5 meters reveal an interesting pattern of relatively thick paleosol horizons compared to the loess intervals. These paleosol horizons even show typical stratigraphic susceptibility patterns easily recognizable across the Danube loess-paleosol sequences covering the LGC (Marković et al., 2015).

3.6. Conclusions

Following a multi-proxy sedimentological and chronological investigation we show that for the uppermost 4.5 m of the loess-paleosol sequence exposed at Kurortne, the lowermost loess unit dated here prior to 123±10 ka and corresponding to the Dnipro unit (equivalent to L2LL1; Marković et al., 2015) was succeeded by the formation of a thick interglacial-type chernozem paleosol, OSL dated in its upper part to 85.0±6 ka (the Kaydaky unit, corresponding to S1SS2).

The Pryluky paleosol (corresponding to S1SS1) overlain by the Uday loess unit which is dated here to 61.2±3.9 ka, is strongly enriched in carbonates, depleted in humus, with lower magnetic susceptibility values and a less abundant <2 μm grain-size fraction than in the Kaydaky paleosol. These data support previously reported observations that the paleosol(s) comprised within the Pryluky unit most likely correspond to interstadial events of the early glacial (with lower chemical weathering indices than the underlying interglacial soil), and the whole Kaydaky-Pryluky sequence is correlative of MIS 5.

The Vytachiv paleosol (i.e., L1SS1) is positioned between the Uday loess (L1LL2, dated here to 61.2±3.9 ka and thus corresponding to MIS 4) and the Bug loess (L1LL1, dated here to 25.8±1.7 ka, and thus pertaining to the upper pleniglacial MIS 2) both characterized by low magnetic susceptibility values denoting loess accumulation under stadial conditions. The Vytachiv paleosol, OSL dated towards the top to 37.7±2.4 ka is represented by a calcaric cambisol with magnetic susceptibility values and proportions of <2 μm particles slightly higher than in the loess. These facts, as well as morphological features indicate that it represents an interstadial(s) formed during the middle pleniglacial (MIS 3).

The Late Pleistocene Prychornomorya loess unit dated at Kurortne between 13.8±3.9 ka and 11.7±0.8 ka (the Late Glacial, the last part of MIS 2) is represented by the carbonate horizon of the Holocene soil. The intense pedogenesis during the Holocene interglacial resulted in the formation of a chernozem soil subtype 'common', which is typical S0 soil in the studied region of Ukraine.

The results discussed here based on integrating luminescence dating with multi-proxy sedimentological data for Kurortne LPS unequivocally ascertain to the LGC the uppermost 4.5 m of the section comprising the interval between first major paleosol (i.e., Kaydaky unit) and the Holocene S0 topsoil. This correlation fully supported by the OSL data helps in clarifying local chronostratigraphic correlations, establish more secure reconstructions of Late Pleistocene environmental changes in the northern Black Sea area, and test the correspondence with the Danube loess chronostratigraphic framework as discussed in Marković et al. (2015).

4. Short-term soil formation events in last glacial east European loess, evidence from multi-method luminescence dating - based on Veres et al. (2018)

4.1. Introduction

Stayky loess-paleosol sequence (LPS) (**Fig. 4.1a-b**) has been documented within the Bug loess unit a record of past rapid climate variability expressed as the alternation of loess beds and several thin, incipient or embryonic soils, ES (**Fig. 4.1c-d**) (Gerasimenko, 2006; Gerasimenko and Rousseau, 2008; Rousseau et al., 2011). Gerasimenko and Rousseau (2008) identified six ES at Stayky northern quarry sequence (N-Stayky), and Rousseau et al. (2011) reported later on twelve distinct ES within the Bug loess at the same site (**Fig. 4.1d**). Kadereit and Wagner (2014) questioned the proposed chronological setting and correlation of embryonic soils with Greenland Interstadial (GI) events because of insufficient dating of Stayky LPS provided by Rousseau et al. (2011). Results of multi-method luminescence investigations of fifteen samples (**Fig. 4.1d-e**) are reported for Stayky LPS in this work, in order to substantiate the chronology. Optically stimulated luminescence (OSL) dating has been applied on all samples, alongside post infrared-infrared stimulated luminescence (pIR-IRSL) dating. The results obtained allow a more comprehensive chronological overview of the Stayky LPS than previously achieved.

4.2. Materials and Methods

4.2.1. The N-Stayky profile and sample collection

The N-Stayky LPS is located in northern Ukraine, south of Kyiv (50°05.65′ N, 30°53.92′ E) on the right bank of Dnieper river (**Fig. 4.1a-b**). Fifteen samples were collected for luminescence dating in 6-cm wide and 10-cm long steel tubes from a section parallel to that of Rousseau et al. (2011) (**Fig. 4.1c-e**). These two sections could differ slightly, but the stratigraphy from Pryluky (pl) unit to the top is very similar (**Fig.4.1b-d**).

4.2.2. Luminescence dating

4.2.2.1. Preparation of luminescence samples

Fifteen samples were collected for luminescence dating from N-Stayky LPS in order to isolate different grain sizes of quartz (4-11 µm, 63-90 µm and 180-250 µm) and fine grained (4-11 µm) polymineral fraction.

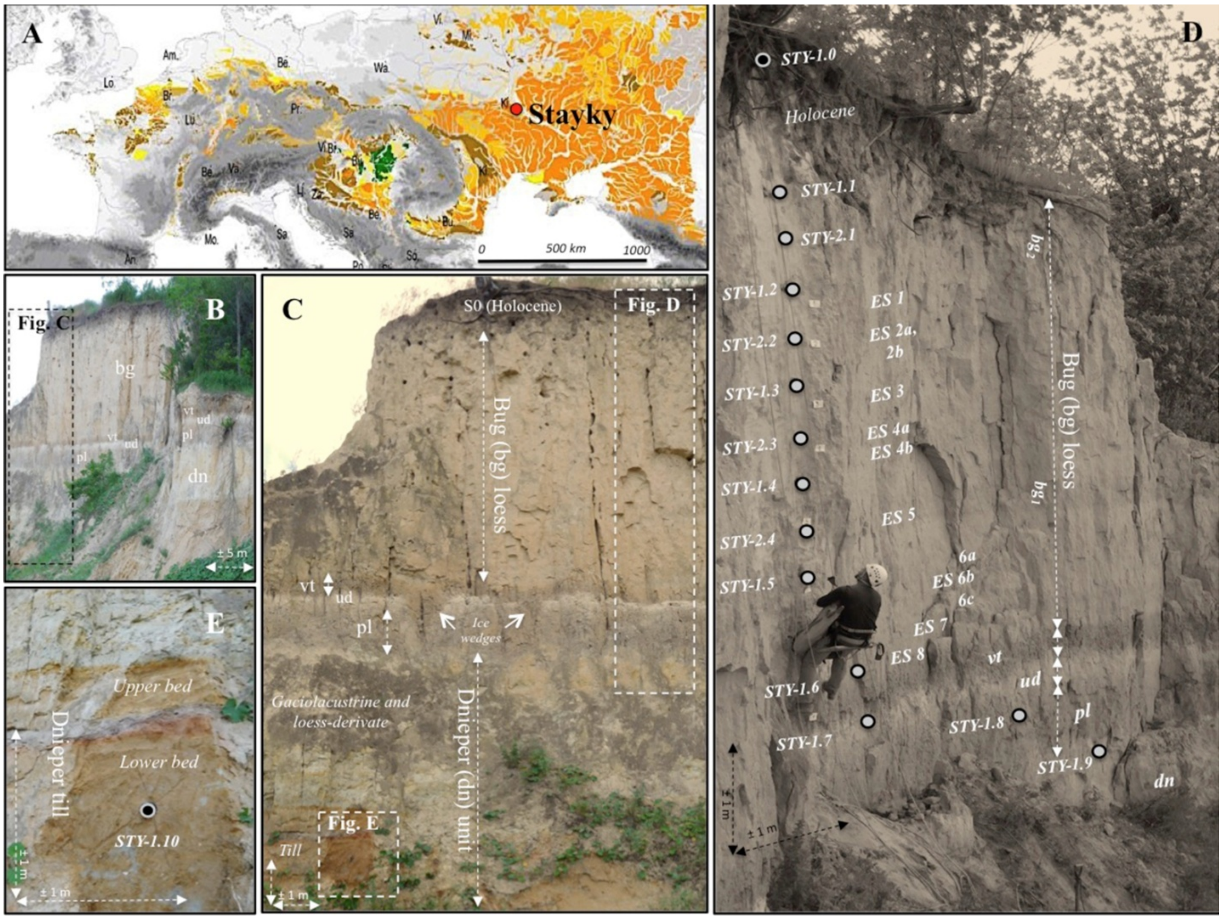

Figure 4.1. Schematic representation of loess distribution in Europe (adapted from Haase et al., 2007) and location of Stayky in eastern Europe **(a)**; The loess-paleosol profile at N-Stayky section near Kiev, northern Ukraine **(b)**; Close-up view of the N-Stayky loess-paleosol profile, and distribution of main lithostratigraphic units discussed in the text **(c)**; The down-wall distribution of OSL samples in relation to the embryonic soils (ES) and other chronostratigraphic units discussed in the text. The height of the sampled sequence is around 10 m **(d)**; Close-up image of the Dnieper till and the location of sample STY-1.10 **(e)**.

For quartz analysis, the purity of the grains extracted was evaluated on all aliquots measured using OSL IR depletion tests (Duller, 2003). The high purity of quartz extracts has been also confirmed by scanning electron microscopy (SEM) and chemical analysis of local area by energy dispersive X-ray spectroscopy (EDX). Such data have been obtained for two samples, STY-1.0 collected from the Holocene soil and STY-1.1 collected from the Bug (bg_2) loess. For both samples, other elements except O and Si (Al for STY-1.0 and Al, Na, Mg for STY-1.1) make up only 0.2% and 1.1%, respectively, indicating that the extracts are very clean, consisting almost exclusively of quartz and that any muscovite or feldspars contamination is negligible.

4.2.2.2. Optically Stimulated Luminescence (OSL) and post infrared infrared stimulated luminescence (pIR-IRSL) measurements

Luminescence measurements were carried out using an automated Risø TL/OSL-DA-20 reader, equipped with blue and infrared light diodes emitting at 470±30 nm and 875±80 nm, respectively. Luminescence investigations were carried out on fine (4-11 µm) and coarse (63-90 µm; 180-250 µm) quartz using the single-aliquot regenerative dose (SAR) protocol (Murray and Wintle, 2000; 2003; Wintle and Murray, 2006). Equivalent doses for polymineral fine 4-11 µm grains were determined using the post infrared-infrared stimulated luminescence pIR-$IRSL_{290}$ protocol (Thiel et al., 2011; Buylaert et al., 2011; 2012). The multi-elevated-temperature pIR-IRSL (MET-pIRIR) protocol (Li and Li, 2011) was also applied on a selection of polymineral fine grain samples (STY-2.4, STY-1.8 and STY 1.9). The modified version of the MET-pIRIR protocol suggested by Fu and Li (2013) that implies the preheat to 200 °C coupled with repeated stimulation in steps of 30 °C up to 170 °C for 100 s was further applied on sample STY-1.0 collected from the Holocene soil.

4.2.2.3. Dose rate determination

The specific activities of radionuclides (^{238}U, ^{232}Th, ^{40}K) were measured by high-resolution gamma spectrometry. Measurements were performed twice using two detectors (Planar and Well detectors). Due to the highly comparable results, in the following only ages obtained through the 'well detector' data are being discussed and the dosimetric information used in age estimations is given in **Table 4.4**. The dose rates were derived based on the conversion factors reported by Guérin et al. (2011).

4.3. Results and Discussion

4.3.1. Performance of the measurement protocols

For suitability of the SAR-OSL protocol for equivalent dose (D_e) estimation of these particular samples was tested in terms of recycling, IR depletion and recuperation tests. For each investigated sample, between 10 and 13 replicate measurements of the equivalent dose were performed. None of the investigated aliquots in this study have been rejected due to, for example, poor recycling, IR depletion or recuperation values, which testifies for the good performance of the quartz extracted from all samples. The equivalent doses were determined by projecting the sensitivity corrected natural OSL signal onto the dose response curve constructed in each case. The growth of the OSL signal was described by the sum of two saturating exponential functions.

Dose recovery test (Murray and Wintle, 2003) was conducted to investigate the reliability of the equivalent doses obtained by applying the SAR protocol on fine and coarse quartz grains from samples STY-2.3 and STY-1.7. A very good recovered to given dose ratio were obtained in all cases (**Table 4.1**)

Table 4.1. Dose recovery test results obtained for the fine (4-11 μm) and coarse (63-90 μm) quartz grains from two samples. n denotes the number of used aliquots.

Sample code	Grain size (μm)	n	Given dose (Gy)	Recovered dose (Gy)	Recovered dose/Given dose
STY-2.3	4-11	4	60	61	1.02 ± 0.01
	63-90	4	48	45	0.93 ± 0.01
STY-1.7	4-11	4	125	124	0.99 ± 0.02
	63-90	4	101	95	0.94 ± 0.01

The variation in equivalent dose as a function of preheat temperature was investigated. A 180 °C cutheat (test dose preheat) was used throughout the measurements. As shown in the **Figure 4.2**, the plateau observed validates the choice of a 220 °C preheat temperature.

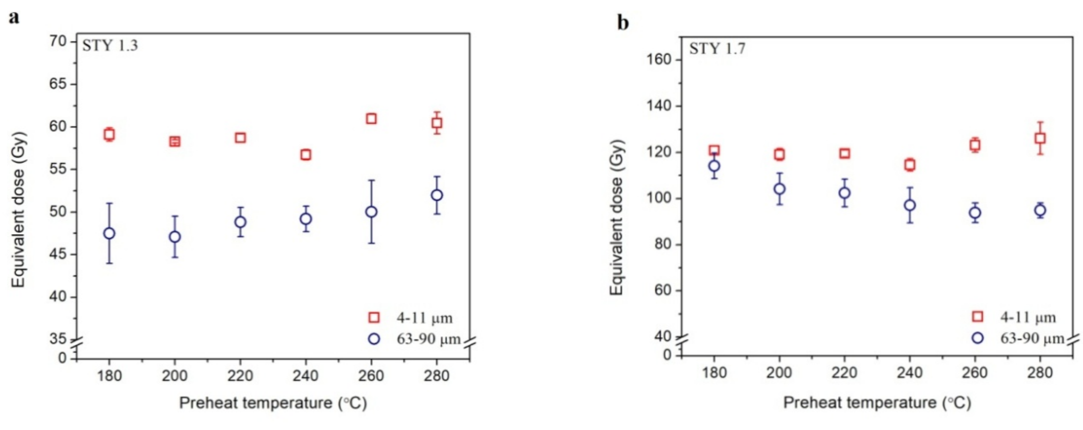

Figure 4.2. Equivalent dose dependence on preheat temperatures for fine (4-11 μm) and coarse (63-90 μm) quartz fractions from samples: a) STY-1.3, and b) STY-1.7.

The equivalent doses of ten polymineral fine-grained (4-11 μm) samples (STY-1.0, 1.2, 2.2, 2.4, 1.5, 1.6, 1.7, 1.8, 1.9 and STY-1.10) were measured by applying the post infrared

infrared stimulated luminescence (pIR-IRSL) using between eight and ten aliquots for each sample. A summary of the equivalent dose values (residuals subtracted) for pIR-IRSL$_{290}$ as well as for the values obtained using the preceding IR$_{50}$ measured signal is presented in **Table 4.4**. For residual dose estimation three aliquots of each sample were exposed to daylight for 22 days and then the residual doses were measured using the same parameters as in case of equivalent dose measurements.

As the pIR-IRSL$_{290}$ protocol was originally designed for dating old samples the modified, less stringent temperature MET-pIRIR protocol suggested by Fu and Li (2013) was applied for STY-1.0 polymineral fine grains. The results are presented in **Figure 4.3 panel a**. It can be seen that a plateau is not reached and the equivalent doses increase as function of stimulation temperature.

A dose recovery test was applied to seven samples to test whether a given dose can be recovered using the pIR-IRSL protocol. Three natural aliquots per sample were bleached under daylight. The aliquots were then given a beta dose similar to the measured D_e for that sample and the given dose measured. A satisfactory recovered to given dose ratio was obtained for samples with equivalent doses up to 200 Gy. For a given dose of 460 Gy (sample STY-1.8) an overestimation of 20% was observed, while in the case of a given dose of 616 Gy (sample STY-1.9) the overestimation is even more significant, amounting to 40%. The results are presented in the **Table 4.2**.

Table 4.2. Dose recovery test results obtained for the pIR-IRSL$_{290}$ signals of polymineral fine grains (4-11 μm) from seven samples. n denotes the number of used aliquots. The residual doses were subtracted.

Sample code	Grain size (μm)	n	Given dose (Gy)	Recovered dose (Gy)	Recovered dose/Given dose
STY-1.0	4-11	3	51	49	0.98 ± 0.04
STY-2.4	4-11	3	89	97	1.10 ± 0.03
STY-1.5	4-11	3	97	102	1.05 ± 0.03
STY-1.6	4-11	4	115	124	1.07 ± 0.06
STY-1.7	4-11	4	188	204	1.09 ± 0.01
STY-1.8	4-11	7	460	552	1.20 ± 0.04
STY-1.9	4-11	4	616	881	1.43 ± 0.04

In order to test the accuracy of the pIR-IRSL$_{290}$ equivalent doses, we applied the multi elevated temperature pIR-IRSL protocol (MET-pIRIR) (Li and Li, 2011) on polymineral fine grains (4-11 µm) of samples STY-2.4, STY-1.8, and STY-1.9 respectively. The results are presented in **Figure 4.3** (panels b, c and d).

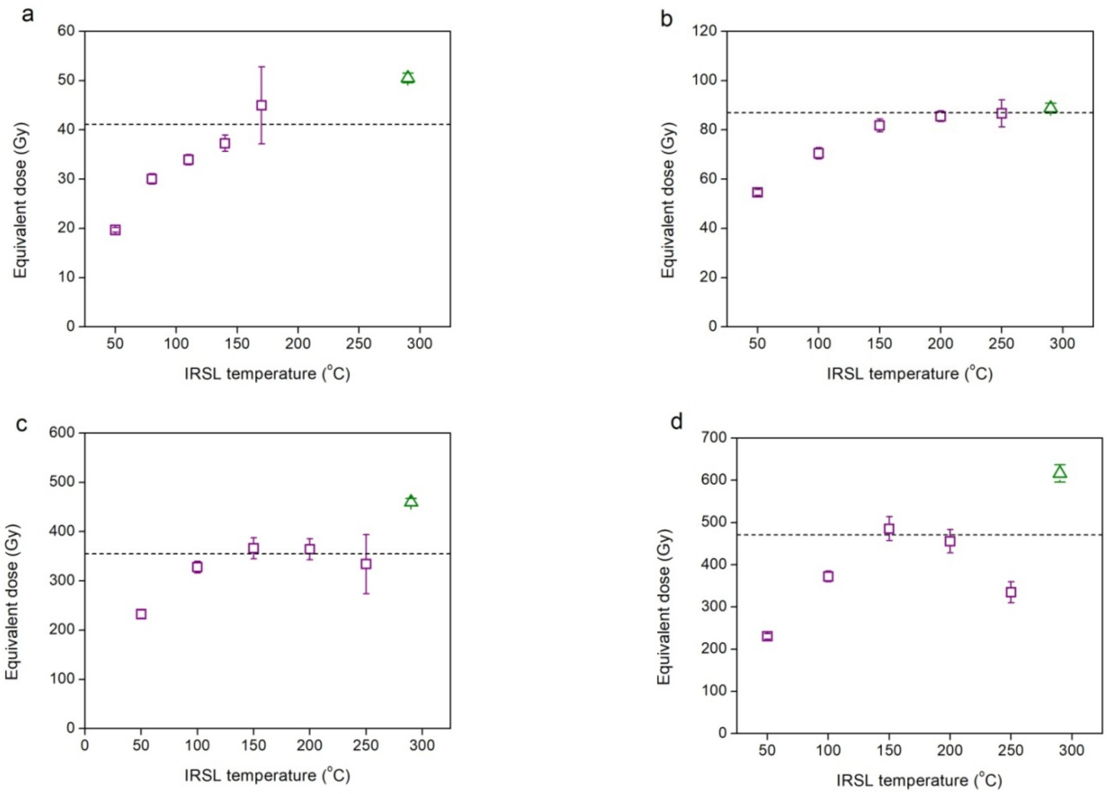

Figure 4.3. Equivalent doses of: a) STY-1.0 polymineral fine grains (4-11 µm) sample obtained using the MET-pIRIR protocol for stimulations of 50 °C-170 °C (purple squares), b) STY-2.4, c) STY-1.8, and d) STY-1.9 polymineral fine grains (4-11 µm) samples obtained using the MET-pIRIR protocol for stimulations of 50 °C-250 °C (purple squares). The equivalent dose obtained using the pIR-IRSL$_{290}$ protocol is also depicted on the graph (green triangle).

4.3.2. Further investigations on the reliability of the equivalent doses obtained in the high dose range

We further examined the laboratory saturation characteristics of OSL and pIR-IRSL$_{290}$ signals by constructing extended SAR dose response curves using 3-4 aliquots of sample STY-1.10 (**Fig. 4.4**).

The growth of the signal with dose is best represented by the sum of two single saturating exponential functions, i.e. $I(D) = I_0 + A(1 - \exp(-D/D_{01})) + B(1 - \exp(-D/D_{02}))$, where I is the intensity of the signal for a given dose D, I_0 is the intercept, A and B are the saturation intensities of the two exponential components and D_{01}, D_{02} are the dose levels characteristic of the dose–response curve of each exponential function (Wintle and Murray, 2006).

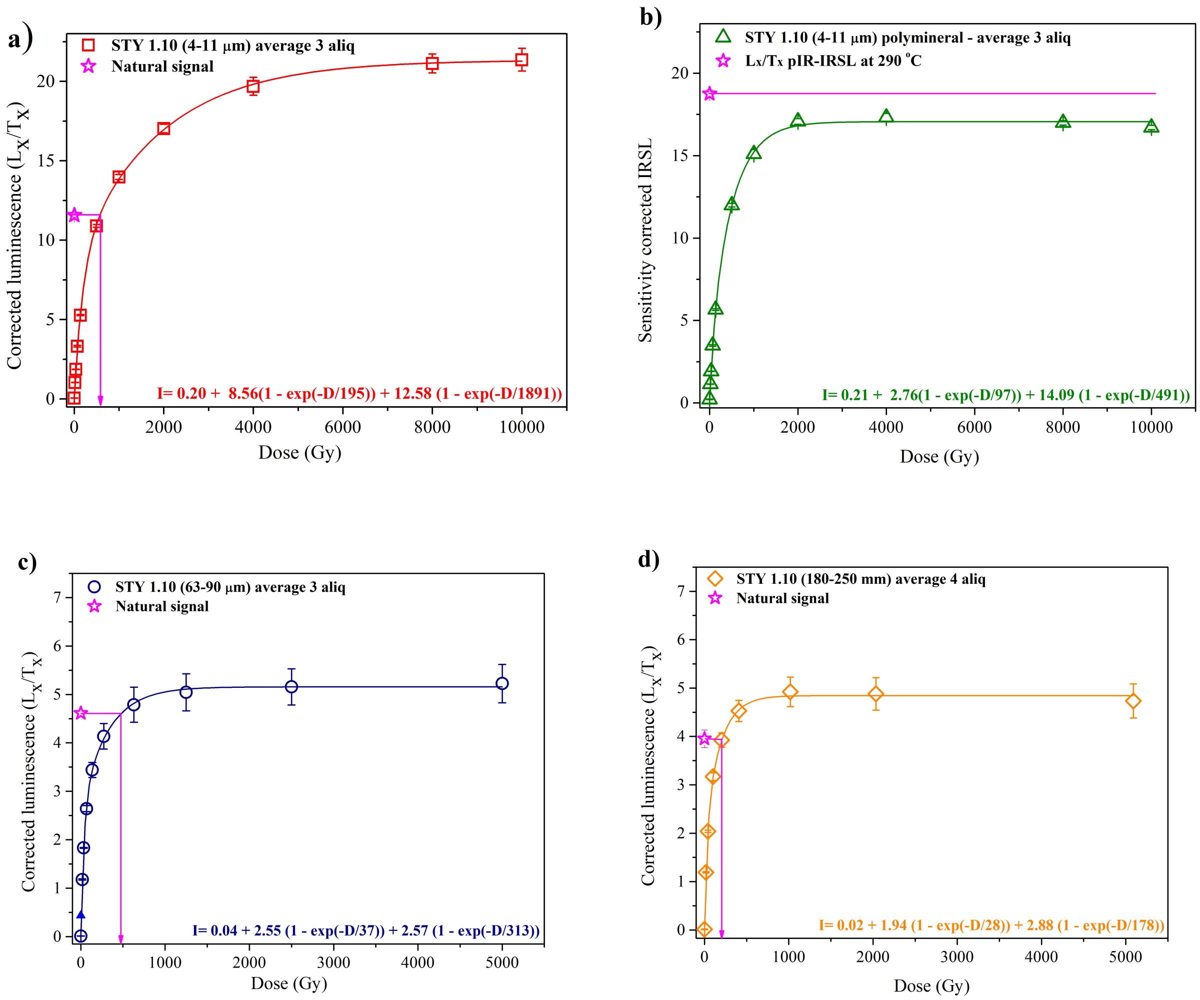

Figure 4.4. Comparison between extended dose-response curves constructed for sample STY-1.10 using a) fine 4–11 µm quartz grains, b) 4–11 µm polymineral fine grains pIR-IRSL$_{290}$ signals, c) coarse 63–90 µm and d) 180–250 µm quartz grains. A test dose of 17 Gy was used throughout the measurements.

From data presented in **Figure 4.4** it can be observed that the fine quartz fraction (4-11 µm) saturates at significantly higher doses than coarse (63-90 µm and 180-250 µm) fractions.

Previous studies on loess samples from the Carpathian Basin, Lower Danube area, or the Chinese Loess Plateau (Timar-Gabor et al., 2012; 2015; 2017) reported similar results regarding the different saturation characteristics of fine and coarse quartz grains. The saturation characteristics of fine quartz OSL signals seem to be higher than the saturation characteristics of the pIR-IRSL$_{290}$ signal (**Fig. 4.4ab**).

By comparing the normalised natural light levels to laboratory saturation light levels it can be noted that in case of both coarse quartz fractions (63-90 µm and 180-250 µm, respectively) the natural OSL signal is close to saturation, exceeding the 85% limit suggested by Wintle and Murray (2006) (**Fig. 4.4cd**), while for fine quartz natural OSL signals are found below saturation (**Fig. 4.4a**).

We have irradiated the 4-11 µm quartz fraction of sample STY-1.10 (natural sensitivity corrected signal denoted as L_n/T_n) with a beta dose of 3500 Gy on top of the natural dose that corresponds to an equivalent dose of 556 Gy, and further compared the luminescence response (denoted as L_n^*/T_n^*) to the response following a regenerative beta dose of 4000 Gy (denoted as L_x/T_x). A very small underestimation is reported (ratio of 0.96±0.04), but within errors, the ratio is consistent to unity (**Table 4.3**). The same experiment was performed on the STY-1.10 63-90 µm quartz where a dose of 492 Gy was added on top of the natural accrued dose.

Table 4.3. The effect of adding large doses on top of the naturally accrued dose for sample STY-1.10. n denotes the number of aliquots used.

Sample code	**Grain size (µm)**	**Equivalent dose (Gy)**	**L_n/T_n**	**Given dose (Gy)**	**n**	**L_n^*/T_n^***	**L_x/T_x**	**L_n^*/T_n^*/ L_x/T_x**
STY-1.10	4-11	556 ± 9.5 (n=13)	11.1 ±0.1 (n=13)	Nat + 3500	5	17.7 ± 0.7		0.96 ± 0.04
				4000	5		18.5 ± 0.1	
	63-90	492 ± 30.4 (n=11)	4.6 ± 0.2 (n=11)	Nat + 492	5	5.1 ± 0.5		1.00 ± 0.13
				1001	5		5.1 ± 0.4	

The obtained ratio between L_n^*/T_n^* and L_x/T_x is consistent to unity (**Table 4.3**) showing that any improperly corrected dose dependent sensitivity change during the first measurement cycle is not relevant in the case of these samples. On the other hand, for fine quartz grains, the observed corrected signal increase with added dose from 11.1±0.1 (L_n/T_n) to 17.7±0.7 (L_n^*/T_n^*). This implies that if the signals of this sample were in field saturation, there is the possibility of some sort of dose dependent instability, either thermal or athermal affecting the signal, or a dose rate dependent sensitivity change in the case of high doses range affecting the laboratory dose response.

4.3.3. Luminescence ages

The OSL ages obtained using two different grain sizes of quartz (4-11 µm and 63-90 µm respectively), along with the IR_{50} and pIR-$IRSL_{290}$ ages calculated using different scenarios for the water content are presented in **Table 4.4**. From **figure 4.5** it can be observed that all ages increase with depth. For the Holocene sample (STY-1.0), the pIR-$IRSL_{290}$ age (**Table 4.4**) obtained overestimate the OSL ages on fine (5.3±0.5 ka) or coarse (4.4±0.4 ka) quartz. This is expected based on the behavior reported in the MET-pIRIR (Fu and Li, 2013) protocol (**Figure 4.3a**) and the comparison of these results to the pIR-$IRSL_{290}$ equivalent doses.

The pIR-$IRSL_{290}$ ages (~16.9-29.5 ka) obtained for samples STY-1.2 to STY-1.6 are in agreement within error limits with the OSL fine and coarse quartz ages (~16.3-25.0 ka) and give us confidence in the general reliability of our multi-methods results in this age range. The OSL ages obtained on quartz for samples STY-1.8 and STY-1.9 are underestimating the pIR-$IRSL_{290}$ ages (**Table 4.4**). In general we consider the pIR-IRSL chronology more reliable than the quartz SAR-OSL ages in the case of samples STY-1.8 to STY-1.10.

The IR_{50} ages obtained for all samples (**Table 4.4**) appear underestimated. We attribute this to the fact that the infrared stimulated luminescence (IRSL) signal is hampered by anomalous fading (Wintle, 1973; Huntley and Lamothe, 2001). As such, the IR_{50} ages will not be discussed further in data interpretation.

In **Table 4.4** and **Figure 4.5** the luminescence ages are reported using both the 'measured' and an 'assumed' water content of 15% for all samples. The rationale behind this approach is twofold. First, while the 'measured' water content is usually considered in luminescence dating, a 15% water content was assumed previously for IRSL dating at Stayky (Rousseau et al., 2011). While past water content variations are hard to quantify, it is very likely that the moisture content was much higher in the past than the one found while sampling the exposed loess wall at N-Stayky. Second, as contradictory chronostratigraphic inferences have been made concerning the comparison of N-Stayky with other records (Rousseau et al., 2011; Kadereit and Wagner, 2014), the chronological data must be critically considered for unambiguous comparison of paleoclimate events.

Table 4.4. Summary of the IRSL at 50 °C , pIR-IRSL at 290 °C and OSL ages obtained on polymineral fine (4-11 µm) grains, fine (4-11 µm) and coarse (63-90 µm) quartz and dosimetry data. The ages for IRSL at 50 °C as well as pIR-IRSL at 290 °C are not corrected for anomalous fading. The uncertainties associated with the luminescence and dosimetry data are random; the uncertainties mentioned with the optical ages are the overall uncertainties. n denotes the number of accepted aliquots; The systematic errors taken into account include: 2% beta source calibration, 3% conversion factors, 5% attenuation and etching factors, 3% gamma spectrometer calibration, 15% cosmic radiation, 25% water content, 50% alpha efficiency values. All uncertainties represent 1σ. Specific activities were measured on Well detector and the ages were determined considering the "measured water " as well as water content assumed to be 15%; measured water content was based on the difference between the as found and the oven-dried weight of the sample; beta attenuation and etching factor used for 63-90 µm quartz was 0.94 (Mejdahl, 1979); adopted alpha efficiency factor was 0.04 for 4-11 µm quartz and 0.08 for polymineral 4-11 µm fine-grains, respectively (Rees-Jones, 1995). The total dose rate consists of the contribution from the beta and gamma radiations for coarse grains as well as the contribution from alpha radiations in the case of fine grains. The contribution of cosmic radiation was taken into account and calculated accordingly to Prescott and Hutton 1994. For coarse quartz grains an internal dose rate of 0.01 ± 0.002 Gy/ka was considered (Vandenberghe et al., 2008).

Sample code	Depth (cm)	U-Ra (Bq/kg)	Th (Bq/kg)	K (Bq/kg)	Meas. water content (%)	Grain size (µm)		De (Gy)	Total dose rate (Gy/ka)		Age (ka)	
									Measured water content	15% water	Measured water content	15% water
STY 1.0	37	32.9 ± 1.4	30.9 ± 1.9	516 ± 19	12.7	4-11	quartz	17.0 ± 0.1 (n = 10)	3.25 ± 0.07	3.18 ± 0.07	5.2 ± 0.4	5.3 ± 0.5
							pIRIR$_{290}$	43 ± 1.1 (n=10)	3.60 ± 0.08	3.52 ± 0.08	11.9 ± 1.0	12.2 ± 1.1
							IR$_{50}$	27.9 ± 1.3 (n=10)	3.60 ± 0.08	3.52 ± 0.08	7.7 ± 0.7	7.9 ± 0.7
						63-90	quartz	12.1 ± 0.5 (n=10)	2.79 ± 0.06	2.73 ± 0.06	4.4 ± 0.4	4.4 ± 0.4
STY 1.1	177	24.8 ± 3.8	30.7 ± 1.4	558 ± 19	2.8	4-11	quartz	56.0 ± 0.4 (n = 10)	3.48 ± 0.11	3.05 ± 0.09	16.1 ± 1.4	18.3 ± 1.6
						63-90	quartz	45.6 ± 1.5 (n=10)	3.00 ± 0.09	2.65 ± 0.08	15.2 ± 1.1	17.2 ± 1.4
STY 2.1	230	28.0 ± 0.6	35.1 ± 1.0	574 ± 16	1.9	4-11	quartz	57.1 ± 0.5 (n = 10)	3.75 ± 0.06	3.26 ± 0.05	15.2 ± 1.3	17.5 ± 1.5
						63-90	quartz	41.6 ± 1.0 (n=10)	3.21 ± 0.05	2.8 ± 0.05	12.9 ± 0.8	14.8 ± 1.1
STY 1.2	277	29.3 ± 1.2	34 ± 1.4	639 ± 18	2.2	4-11	quartz	56.2 ± 0.3 (n = 10)	3.96 ± 0.08	3.45 ± 0.07	14.2 ± 1.2	16.3 ± 1.3
							pIRIR$_{290}$	64.1 ± 2.1 (n=10)	4.36 ± 0.08	3.79 ± 0.07	14.7 ± 1.3	16.9 ± 1.5
							IR$_{50}$	41.4 ± 1.1 (n=10)	4.36 ± 0.08	3.79 ± 0.07	9.5 ± 0.8	10.9 ± 0.9
						63-90	quartz	44.3 ± 1.7 (n=10)	3.41 ± 0.07	2.98 ± 0.06	13.0 ± 0.9	14.9 ± 1.2
STY 2.2	330	31.0 ± 0.9	24.5 ± 0.6	551 ± 19	1.8	4-11	quartz	57.5 ± 0.5 (n = 10)	3.48 ± 0.07	3.02 ± 0.06	16.5 ± 1.4	19.0 ± 1.6
							pIRIR$_{290}$	70.6 ± 2.3 (n=10)	3.84 ± 0.07	3.32 ± 0.06	18.4 ± 1.6	21.3 ± 1.8
							IR$_{50}$	37.9 ± 1.8 (n=10)	3.84 ± 0.07	3.32 ± 0.06	9.9 ± 0.9	11.4 ± 1.1
						63-90	quartz	44.2 ± 1.0 (n=10)	2.99 ± 0.06	2.61 ± 0.05	14.8 ± 0.9	16.9 ± 1.3

Sample code	Depth (cm)	U-Ra (Bq/kg)	Th (Bq/kg)	K (Bq/kg)	Meas. water content (%)	Grain size (µm)		De (Gy)	Total dose rate (Gy/ka)		Age (ka)	
									Measured water content	15% water	Measured water content	15% water
STY 1.3	379	33.2 ± 0.7	34.5 ± 1.6	578 ± 19	1.9	4-11	quartz	59.6 ± 0.5 (n = 10)	3.87 ± 0.08	3.35 ± 0.07	15.4 ± 1.4	17.8 ± 1.5
						63-90	quartz	46.8 ± 1.1 (n=10)	3.29 ± 0.07	2.87 ± 0.06	14.2± 0.9	16.3 ± 1.2
STY 2.3	437	28.5 ± 0.8	22.5 ± 0.6	505 ± 17	2.9	4-11	quartz	59.6 ± 0.5 (n = 10)	3.15 ± 0.06	2.77 ± 0.05	18.9 ± 1.6	21.5 ± 1.8
						63-90	quartz	47.9 ± 1.0 (n=10)	2.71 ± 0.06	2.39 ± 0.05	17.7 ± 1.1	20.0 ± 1.5
STY 1.4	487	35.8 ± 2.3	33.5 ± 1.8	620 ± 20	9.0	4-11	quartz	64.0 ± 0.6 (n = 10)	3.73 ± 0.09	3.51 ± 0.08	17.1 ± 1.5	18.2 ± 1.6
						63-90	quartz	53.2 ± 1.6 (n=10)	3.19 ± 0.07	3.0 ± 0.07	16.7 ± 1.2	17.7 ± 1.4
STY 2.4	540	30.2 ± 2.8	35.4 ± 1.1	565 ± 19	5.4	4-11	quartz	69.7 ± 0.8 (n = 12)	3.59 ± 0.09	3.25 ± 0.08	19.4 ± 1.7	21.5 ± 1.9
							$pIRIR_{290}$	79.8 ± 2.7 (n=10)	3.99 ± 0.1	3.59 ± 0.09	20.0 ± 1.8	22.2 ± 2.0
							IR_{50}	55.0 ± 2.2 (n=10)	3.99 ± 0.1	3.59 ± 0.09	13.8 ± 1.3	15.3 ± 1.4
						63-90	quartz	59.7 ± 1.5 (n=10)	3.06 ± 0.07	2.78 ± 0.07	19.5 ± 1.3	21.5 ± 1.7
STY 1.5	587	34.1 ± 0.5	33.9 ± 1.2	530 ± 20	3.0	4-11	quartz	70.5 ± 0.5 (n = 10)	3.64 ± 0.07	3.2 ± 0.06	19.4 ± 1.7	22.1 ± 1.9
							$pIRIR_{290}$	88.5 ± 1.7(n=10)	4.06 ± 0.08	3.56 ± 0.07	21.8 ± 1.9	24.9 ± 2.2
							IR_{50}	52.4 ± 0.9 (n=10)	4.06 ± 0.08	3.56 ± 0.07	12.9 ± 1.1	14.7 ± 1.3
						63-90	quartz	57.6 ± 1.5 (n=10)	3.08 ± 0.07	2.72 ± 0.06	18.7 ± 1.2	21.2 ± 1.6
STY 1.6	687	26.5 ± 0.3	28.7 ± 1.6	652 ± 21	10.5	4-11	quartz	81.7 ± 0.9 (n = 10)	3.42 ± 0.08	3.26 ± 0.07	23.9 ± 2.0	25.0 ± 2.1
							$pIRIR_{290}$	105 ± 2 (n=10)	3.73 ± 0.08	3.56 ± 0.08	28.1 ± 2.3	29.5 ± 2.4
							IR_{50}	66.5 ± 2.4 (n=10)	3.73 ± 0.08	3.56 ± 0.08	17.8 ± 1.6	18.7 ± 1.6
						63-90	quartz	77.1 ± 2.3 (n=10)	2.97 ± 0.07	2.84 ± 0.06	26.0 ± 1.9	27.2 ± 2.2
STY 1.7	767	33.1 ± 0.1	35.6 ± 1.3	472 ± 17	2.2	4-11	quartz	121 ± 2 (n=10)	3.47 ± 0.07	3.02 ± 0.06	34.9 ± 3.3	40.1 ± 3.7
							$pIRIR_{290}$	180 ± 2 (n=10)	3.90 ± 0.07	3.38 ± 0.06	46.1 ± 4.1	53.2 ± 4.6
							IR_{50}	99.8 ± 1.8 (n=10)	3.90 ± 0.07	3.38 ± 0.06	25.6 ± 2.3	29.5 ± 2.6
						63-90	quartz	101 ± 5 (n=10)	2.91 ± 0.06	2.55 ± 0.05	34.6 ± 2.7	39.6 ± 3.5
STY 1.8	870	47.0 ± 1.7	36.1 ± 1.8	497 ± 17	2.0	4-11	quartz	264 ± 2 (n=10)	3.94 ± 0.08	3.42 ± 0.07	66.9 ± 6.4	77.2 ± 7.3
							$pIRIR_{290}$	446 ± 8 (n=10)	4.48 ± 0.09	3.87 ± 0.08	99.6 ± 9.2	115 ± 11
							IR_{50}	266 ± 8(n=10)	4.48 ± 0.09	3.87 ± 0.08	59.5 ± 5.7	68.9 ± 6.5
						63-90	quartz	249 ± 12 (n=11)	3.27 ± 0.07	2.85 ± 0.06	75.9 ± 5.7	87.2 ± 7.5
STY 1.9	930	40.6 ± 0.7	38.8 ± 0.8	548 ± 19	2.2	4-11	quartz	301 ± 2 (n=10)	4.00 ± 0.07	3.47 ± 0.06	75.3 ± 7.0	86.7 ± 7.9
							$pIRIR_{290}$	599 ± 21 (n=10)	4.50 ± 0.07	3.89 ± 0.06	133 ± 13	154 ± 14
							IR_{50}	287 ± 10(n=10)	4.50 ± 0.07	3.89 ± 0.06	63.9 ± 6.0	73.8 ± 6.9
						63-90	quartz	215 ± 11 (n=10)	3.33 ± 0.06	2.91 ± 0.05	64.3 ± 4.9	73.6 ± 6.5
STY 1.10	1200	25.7 ± 0.6	24.3 ± 0.8	329 ± 15	2.3	4-11	quartz	556 ± 10 (n=13)	2.47 ± 0.06	2.15 ± 0.05	225 ± 21	258 ± 24
							$pIRIR_{290}$	-	-	-	-	-
							IR_{50}	531 ± 33 (n=8)	2.79 ± 0.06	2.42 ± 0.05	191 ± 21	220 ± 24
						63-90	quartz	492 ± 30 (n=11)	2.07 ± 0.05	1.81 ± 0.04	237 ± 20	271 ± 26

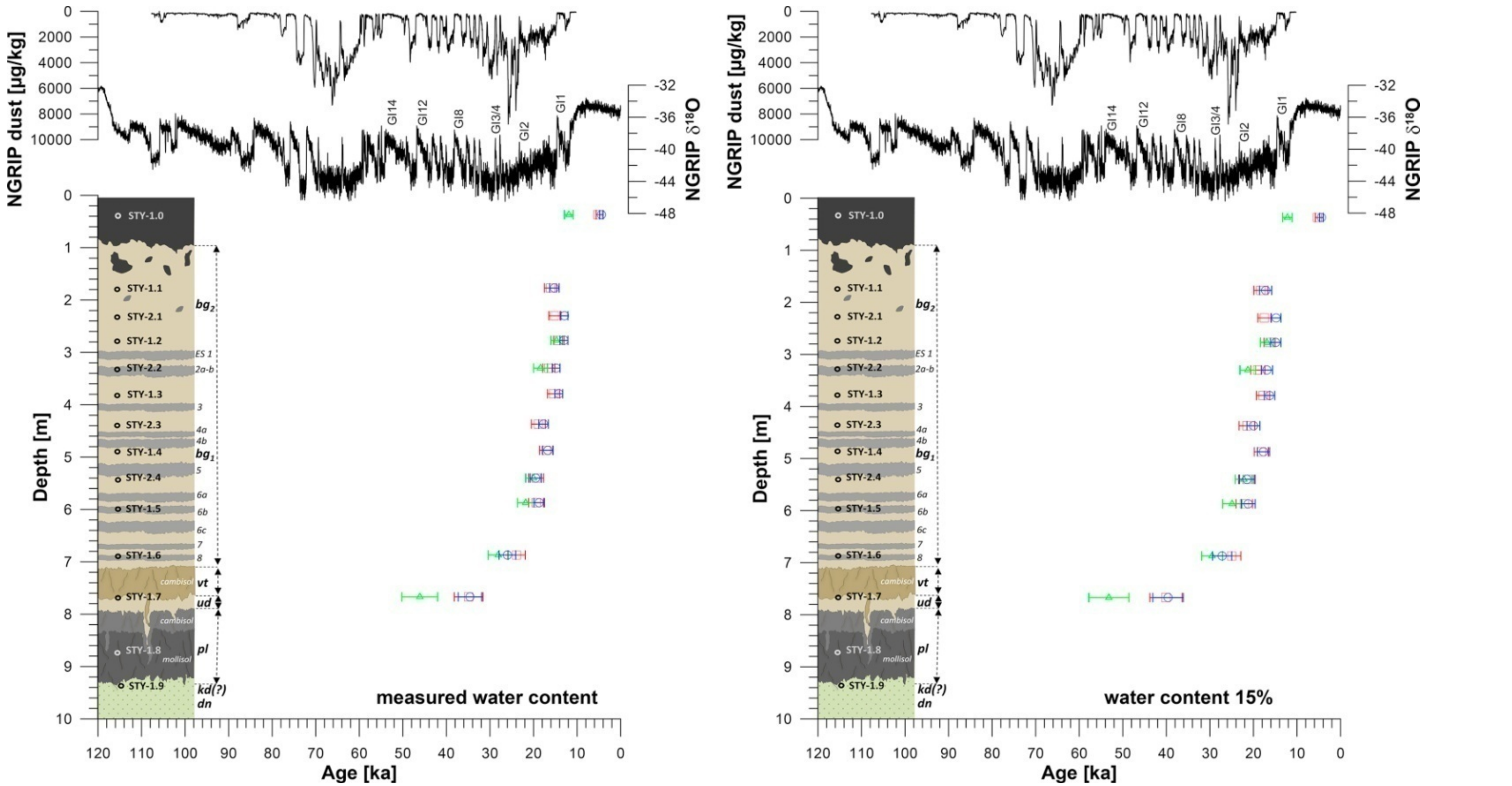

Figure 4.5. Schematic representation of the lithostratigraphy of N-Stayky profile (Rousseau et al., 2011), and the depth distribution of luminescence data (at 1σ) for samples STY-1.0 to STY-1.7 in a comparison with NGRIP $\delta^{18}O$ data and mineral dust data on the GICC05 timescale (Ruth et al., 2007; Svensson et al., 2008). Ages based on 'measured water content' (left panel) and an 'assumed 15% water content' (right panel) for OSL fine grain (4–11 µm) quartz in red squares, OSL coarse grain (60–93 µm) quartz in blue circles, and pIR-IRSL$_{290}$ polymineral grains in green triangles.

4.4. Paleoenvironmental and chronostratigraphic implications

4.4.1. Dating the Dnieper till, Pryluky pedocomplex and Vytachiv paleosol

For sample STY-1.10 collected from the Dnieper till, providing a reliable age was not possible due to the saturation of luminescence signals. The natural signals for pIR-IRSL$_{290}$ were found in saturation and thus the minimum equivalent dose should be ~2000 Gy, corresponding to an age of about 700 ka.

OSL ages of 75.3±7 ka - 86.7±7.9 ka on fine quartz and 64.3±4.9 ka - 73.6±7.5 ka on coarse quartz were obtained for sample STY-1.9 collected from the Cca horizon of Pryluky (pl) mollisol. The pIR-IRSL$_{290}$ dating provided much older ages in the range of 133±13 ka to 154±14 ka, respectively. OSL ages of 66.9±7.4 ka - 77.2±7.3 ka (4-11 µm) and 75.9±5.7 ka - 87.2±7.5 ka (63-90 µm) were obtained for sample STY-1.8 collected from the top half of A1 horizon of Pryluky (pl) mollisol. The pIR-IRSL$_{290}$ dating provided ages of 99.6±9.2 ka to 115±11 ka. Quartz ages based on equivalent doses in this range should be regarded as minimum ages and we consider the pIR-IRSL$_{290}$ data (**Table 4.4**) to be more reliable for these samples.

It is very likely that Vytachiv (vt) cambisol at N-Stayky preserving a very distinctive Cca horizon (Rousseau et al., 2011) relates only to the middle paleosol of the tripartite Vytachiv pedocomplex elsewhere (Gerasimenko, 2006; Bokhorst et al., 2011; Gozhik et al., 2014). Further, Rousseau et al. (2011) IRSL dated the middle part of Vytachiv cambisol at N-Stayky to 30.2±3.1 ka, whereas sample STY-1.7 collected from the Cca horizon close to the transition to the underlying Uday (ud) loess provided OSL ages of 34.9±3.3 ka - 40.1±3.7 ka (4-11 µm) to 34.6±2.7 ka - 39.6±3.5 ka (63-90 µm). The pIR-IRSL$_{290}$ dating returned ages between 46.1±4.1 ka and 53.2±4.6 ka. Sample STY-1.6 from the overlying ES 8 (within Bug loess) provided ages of 23.9±2 ka and 25±2.1 ka for fine quartz, 26.0±1.9 ka and 27.2±2.2 ka for coarse quartz, and respectively 28.1±2.3 ka and 29.5±2.4 ka for pIR-IRSL$_{290}$ dating (**Fig 4.5**).

Albeit the good agreement between the dated quartz grain sizes and the pIR-IRSL$_{290}$ results for STY-1.6 (**Table 4.4**), there is a noticeable difference for STY-1.7, with OSL data indicating middle-to-late MIS 3 ages and pIR-IRSL$_{290}$ data early-to-middle MIS 3 age ranges instead (**Fig 4.5**). Based on luminescence investigations in this age range and results from intrinsic rigour behaviour tests, one cannot assess with certainty whether quartz OSL or feldspars pIR-IRSL$_{290}$ data are more accurate. The age range of STY-1.6 indicates that ES8 formed at the onset of the Late Pleniglacial, at or after the MIS 3/2 transition. Relating the Vytachiv (vt) unit at

N-Stayky with the Greenland event stratigraphy as discussed in Rousseau et al. (2011, 2017) and Kadereit and Wagner (2014) is challenging in the light of existing chronological data and stratigraphic evidence.

4.4.2. The Bug (bg) loess and the pervasive MIS 2 embryonic soils

Sample STY-1.5 from the middle soil bed within ES6 (**Figs 4.1d**) provided OSL fine quartz ages of 19.4±1.7 ka and 22.1±1.9 ka, and 18.7±1.2 ka to 21.2±1.6 ka for coarse quartz. There is an excellent agreement between OSL data and the pIR-$IRSL_{290}$ results in the range of 21.8±1.9 ka and 24.9±2.2 ka.

OSL ages of 19.4±1.7 ka and 21.5±1.9 ka on fine quartz, and 19.5±1.3 ka to 21.5±1.7 ka on coarse quartz were obtained for sample STY-2.4 collected from ES5. The pIR-$IRSL_{290}$ ages of 20.0±1.8 ka and 22.2±2.0 ka are highly comparable with the OSL data (**Table 4.4**). The ages reported here are younger compared to the 27.6±2.7 ka IRSL age previously reported by Rousseau et al. (2011) for the same pedogenetic horizon at N-Stayky.

The dating of seven more samples from STY-1.4 to STY-1.1 (**Figs 4.1d**) comprising six ES horizons (from ES4 to ES1) and the interbedded loess (including sub-unit bg_2) provided very comparable OSL ages in the range of ~19-14 ka or ~21-13 ka depending on the water content used (**Table 4.4**). The pIR-$IRSL_{290}$ ages obtained for several pilot samples further support the OSL results (**Fig 4.5**). The N-Stayky section is capped by the Holocene mollisol with the OSL ages of ~4.0-5.3 ka (STY-1.0) linking the emplacement time of its A1 horizon to mid-Holocene.

The paleoclimate significance of the embryonic soils in the N-Stayky bg_1 loess is intriguing. **Figure 4.5** shows the luminescence data discussed here, alongside comparison with NGRIP $\delta^{18}O$ and mineral dust content (Ruth et al., 2007; Svensson et al., 2008; Rasmussen et al., 2014). As it can be visualized in **Figure 4.5**, all embryonic pedogenetic horizons starting with ES8 would be younger than GI-4, or even GI-3, as chronologically defined in the Greenland ice data (Rasmussen et al., 2014). This is irrespective of the water content used in defining age ranges, or the luminescence method employed (**Table 4.4**). As such, the dating of the Bug loess raises implications concerning both the chronological span of these embryonic soils and the forcing mechanisms that controlled their development.

4.5. Conclusions

Detailed OSL investigations were performed on quartz of different grain sizes and ages collected from the loess-paleosol sequence at N-Stayky, Ukraine. For samples encompassing the Bug loess unit, ages ranging from ~15 ka to ~27/29 ka have been obtained, the investigated quartz grain size fractions (4-11 µm and 63-90 µm) being in perfect agreement. Confidence in the accuracy of these results was increased through pIR-IRSL$_{290}$ dating that supports the OSL chronology for the Bug unit. Deriving a reliable multi-method chronological framework for the Bug loess is critical in the light of previous discussions on the paleoclimate correspondence between a series of embryonic soils and Greenland interstadial rapid climate variability and our multi-method luminescence data demonstrate that these short-term phases of soil formation took place during MIS 2, between ~27-29 to 15 ka. As no corresponding variability is seen in ice core isotope data, the results point to complex hydroclimate variability during the last deglaciation over the mid-latitudes loess fields of Europe that require further investigations.

The dating of Vytachiv paleosol, previously debatably linked to various interstadial events within MIS 3 indicate that it developed during middle-to-late MIS 3. It is thus likely that this part of the Stayky record is either not continuous, or that it encompasses a broader age range within MIS 3 than previously considered; this would not allow for an unambiguous linking of this paleosol with specific GI event(s) as previously suggested.

The pIR-IRSL$_{290}$ dating of the loams immediately underneath Pryluky unit in the range of ~120 ka to ~168 ka and of the Pryluky mollisol from ~90 ka to 126 ka confirm the broad correspondence of this unit with MIS 5, although poor dose recovery results open the possibility for further testing on the degree these ages provide overestimated results as quartz data severely underestimate the pIR-IRSL$_{290}$ ages.

For the sample collected from the Dnieper till, in the case of coarse quartz grains (63-90 µm as well as 180-250 µm) the natural OSL signals were close to saturation (~85% of maximum light level or higher). The pIR-IRSL$_{290}$ signals from the same sample were found to be in saturation. In the case of 4-11 µm quartz, the natural OSL signals were at about 50-60% from the maximum laboratory light levels. Overall, the multi-method luminescence dating of Stayky clarified several previously un-resolved chronostratigraphic issues, suggesting that at least for MIS 2, this record could be considered as a reference site in mid-latitude European loess paleoclimatology.

5. Latest Pleistocene to Holocene loess in the central Great Plains: Optically stimulated luminescence dating and multi-proxy analysis of the Enders and Kuma loess sections (Nebraska, USA) - based on Tecsa et al. (2020b)

5.1. Introduction

This paper presents a detailed optically stimulated luminescence (OSL) chronology as well as multi-proxy analysis obtained for the first time on the Enders and Kuma sections, located in southwestern Nebraska, central Great Plains. A more comprehensive analysis of OSL ages from three grain size fractions (4-11 µm, 63-90 µm and 90-125 µm) and consideration of varying water contents strengthen the chronological basis for interpreting records from these sites. This study provides the first opportunity to test whether the luminescence ages of three different particle size classes are in agreement in important North American loess-paleosol sequences. The loess-paleosol stratigraphy at the Enders site is similar to that observed at the Wauneta site, 12.5 km NNE of Enders. We discuss similarities and differences between the results from Enders and Wauneta sites, distinguishing the regional paleoclimatic signal from effects of local setting, and also compare the loess record of the Pleistocene-Holocene transition from the Great Plains with loess records from Eurasia.

5.2. Study sites and samples

The Enders (40°23' N, 101°28' W) and Kuma (40°28' N, 101°23' W) sites are located in southwestern Nebraska, in the central Great Plains of North America.

Twelve samples were collected for luminescence dating from the topmost 6 meters along two adjacent profiles of the upper and lower parts of the Enders section, with 37 cm of overlap. Paleosols identified visually in the field include the Brady Soil and more weakly developed paleosols in the overlying Holocene loess **(Fig. 5.1)**.

Kuma section is relatively simple in terms of its stratigraphy, compared to the stratigraphy of Enders and Wauneta (**Fig. 5.1**). A thick unit of Peoria loess is capped by modern soil, which is around 1 m thick and clearly separated into genetic horizons (**Fig. 5.1**). At Kuma site, Bignell Loess is missing, so that the Brady soil and the modern soil have merged into a single unit (Kuzila, 1995). Here eight samples were collected for luminescence dating from the topmost 2 meters, closely encompassing the visual L1/S0 transition (**Fig. 5.1**).

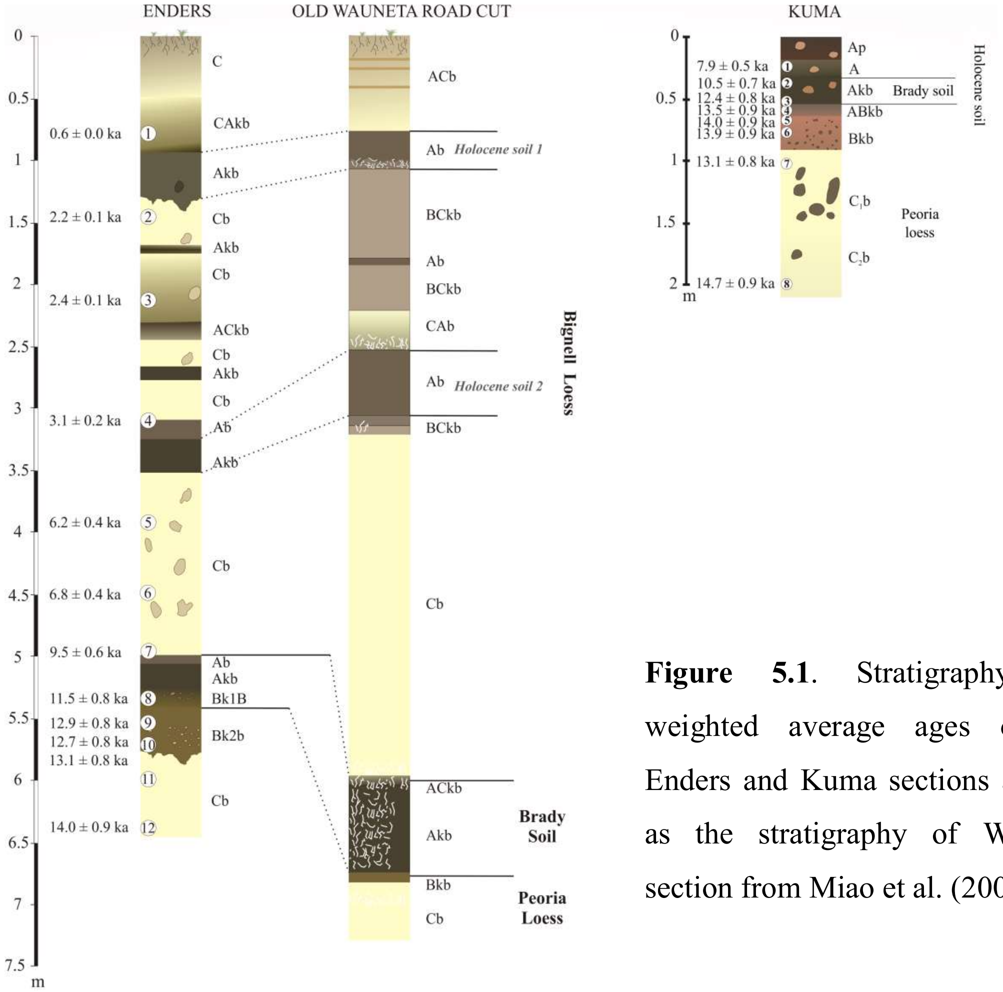

Figure 5.1. Stratigraphy and weighted average ages of the Enders and Kuma sections as well as the stratigraphy of Wauneta section from Miao et al. (2007a).

5.3. Methods and instrumentation

Determinations of magnetic susceptibility and particle size analyses at Enders section were made on 350 sediment samples collected at 2 cm resolution from carefully cleaned outcrop walls. At Kuma site, 49 sediment samples for magnetic susceptibility determinations were collected from a carefully cleaned outcrop wall, at 4 cm resolution.

5.3.1. Magnetic susceptibility

The volumetric magnetic susceptibility was measured at frequencies of 300 Hz (χ_{lf}) and 3000 Hz (χ_{hf}) using a Magnon International VSFM. Frequency dependence of magnetic susceptibility (χ_{fd}) was expressed as a mass-specific loss of susceptibility $\chi_{fd}= ((\chi_{lf} - \chi_{hf})/ \chi_{lf})*100$ (Dearing et al., 1996).

5.3.2. Grain size

Grain-size measurements for samples collected from Enders section were performed using a Malvern Mastersizer 2000MU laser diffraction particle size analyzer. For comparison, samples at 2 cm intervals from a core at Wauneta were reanalyzed by identical methods in the same instrument, since methods used earlier by Miao et al. (2007a) were slightly different.

5.3.3. OSL dating

For luminescence dating, twelve samples were collected from Enders section and eight samples from Kuma site to extract different grain sizes of quartz (4-11 μm, 63-90 μm and 90-125 μm). Measurements were carried out using standard and automated Risø TL/OSL-DA-20 readers equipped with classic or automated detection and stimulation head (DASH) (Lapp et al., 2015). OSL investigations were carried out using the single-aliquot regenerative dose (SAR) protocol for the fine (4-11 μm) and coarse (63-90 and 90-125 μm) fractions (Murray and Wintle, 2000; 2003). The suitability of these samples for equivalent dose determination using the SAR protocol was tested in terms of recycling, infrared (IR) depletion and recuperation tests. The purity of the quartz extracts was evaluated using OSL IR depletion tests (Duller, 2003) on all aliquots measured. None of the investigated aliquots have been rejected due to poor recycling, IR depletion or recuperation values.

The specific activities of radionuclides were measured by means of high resolution gamma spectrometry. The values for radionuclide concentrations as well as the total dose rates for samples collected from Enders and Kuma sections are given in **Tables 5.1-5.2**.

5.4. Results

5.4.1. Grain size and magnetic susceptibility results

Grain size data obtained at Enders section indicate a much higher content of the >63 μm fraction (20-38%) than in typical loess of other regions, also observed at the Wauneta site (Miao et al., 2007a) and indicating short-distance transport in suspension at a low height above ground (Pye, 1987, p. 50-51). The >63 μm fraction is least in the Brady Soil and is somewhat lower in the upper prominent Holocene paleosol (~130-90 cm) than in the rest of the Bignell Loess. There is a proportional increase in the fine <16 μm fraction in both of those soils and the <2 μm fraction also increases in the Brady Soil. At the Wauneta site, the <16 μm fraction is relatively high in the Brady Soil and both major Holocene paleosols, although with significant variation within each paleosol. The most interesting aspect of the grain size profile involves variation just above and within the Brady Soil at Enders and Wauneta sites.

The low-frequency magnetic susceptibility (χ_{lf}) at Enders section varies between 122 10^{-8} m^3/kg and 200 10^{-8} m^3/kg. χ_{lf} is slightly elevated within the Brady Soil, compared to the underlying Peoria Loess and the relatively unweathered Bignell Loess just above it, with some variation among Brady Soil horizons. χ_{fd} shows minor enhancement in the Brady Soil but not in the Holocene paleosols. All of these results are similar to those obtained at the Wauneta site (Figure 4 of Miao et al., 2007a), although the χ_{lf} and χ_{fd} profiles differ in detail between these sites.

The low-frequency magnetic susceptibility (χ_{lf}) at Kuma site varies between 118 10^{-8} m^3/kg and 169 10^{-8} m^3/kg. χ_{lf} shows high values with some variations in the Holocene soil horizons while low values are found in the Peoria loess. The behavior of magnetic susceptibility reflects a gradual transition from the Last Glacial towards the Holocene.

5.4.2. Luminescence properties and equivalent doses

The equivalent doses were determined by projecting the sensitivity corrected natural OSL signal onto the dose response curve constructed in each case. For each investigated sample, between 10 and 20 replicate measurements of the equivalent dose were performed.

Dose recovery test (Murray and Wintle, 2003) was conducted to investigate the reliability of the equivalent doses obtained by applying the SAR protocol on fine (4-11 µm) and coarse (63-90 µm) quartz grains of five samples from Enders section. At Kuma section, the dose recovery test was carried out on coarse (63-90 µm) quartz grains from five samples. As seen in **Figure 5.2**, very good recovery to given dose ratios were obtained in all cases for both sections, indicating that the laboratory doses given prior to any heat treatment are measured with accuracy using the SAR protocol.

The variation in equivalent dose as a function of preheat temperature in combination with a 180 ºC cutheat was also investigated at both sections. As shown in **Figure 5.3**, the plateau observed validates the choice of a 220°C preheat temperature.

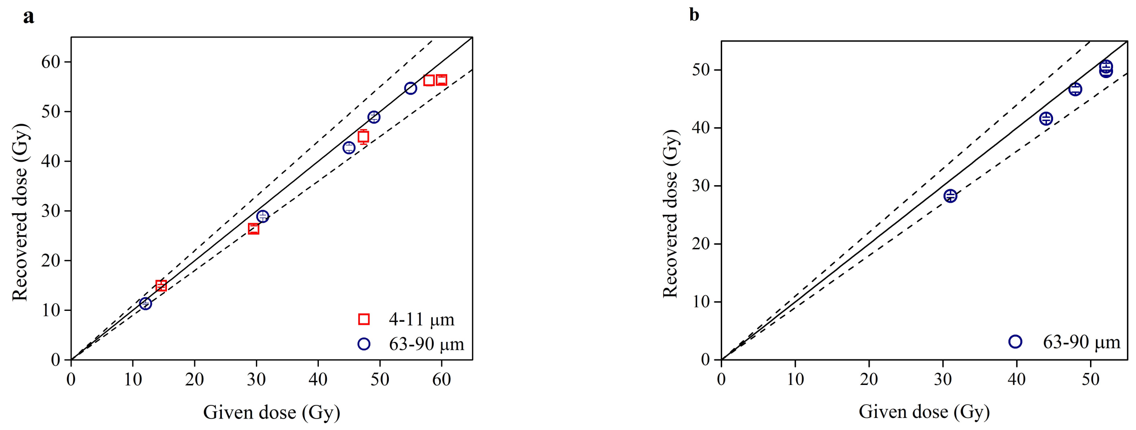

Figure 5.2. (a) Dose recovery test results for fine (4-11 µm) and coarse (63-90 µm) quartz fractions of five samples (END 1.4, END 1.6, END 1.8, END 1.10 and END.12) from Enders section. **(b)** Dose recovery test results for coarse (63-90 µm) quartz fraction of five samples (KUM 1.1-1.5) from Kuma section. The given irradiation doses were chosen to match the equivalent dose of each sample. The solid line indicates the ideal 1:1 dose recovery ratio while the dash lines bracket a 10% variation from unity.

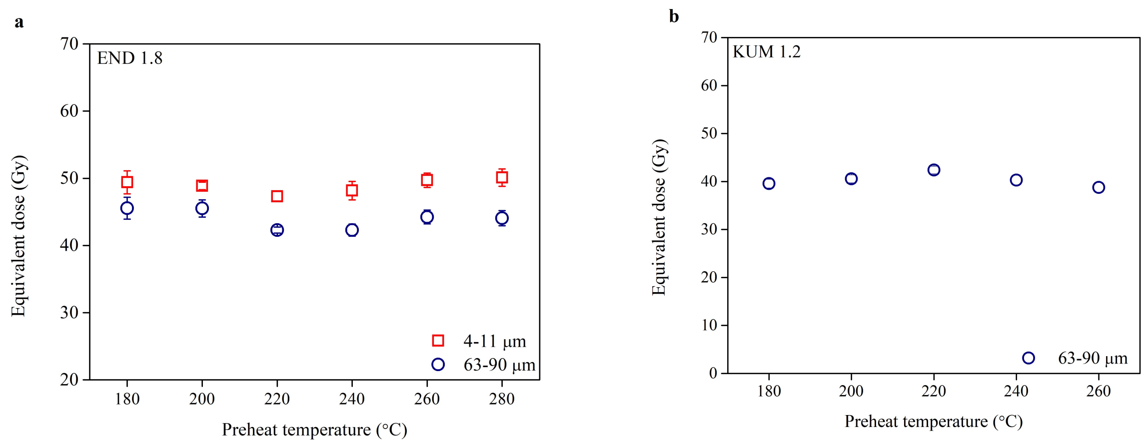

Figure 5.3. (a) Equivalent dose dependence on preheat temperatures for fine (4-11 µm) and coarse (63-90 µm) quartz fractions from sample END 1.8. **(b)** Equivalent dose dependence on preheat temperatures for coarse (63-90 µm) quartz fraction from sample KUM 1.2.

5.4.3. OSL ages

Within uncertainties, optical ages obtained at Enders and Kuma sections are in agreement for all grain sizes of quartz (4-11 µm, 63-90 µm and 90-125 µm) except for the cases of END 1.6 63-90 µm and KUM 1.7 4-11 µm quartz ages, which we consider to be outliers (**Tables 5.1-5.2**).

Table 5.1. Summary of the luminescence and dosimetry data obtained for Enders section. Weighted OSL ages are calculated according to Aitken (1985). The uncertainties associated with the luminescence and dosimetry data are random; the uncertainties mentioned with the optical ages are the overall uncertainties. All uncertainties represent 1σ. The ages were determined considering the "as found" water content, with a relative error of 25%; n denotes the number of accepted aliquots; beta attenuation and etching factor used for 63-90 µm and 90-125 µm fractions are 0.94±0.050 and 0.92±0.050, respectively; adopted alpha efficiency factor was 0.04±0.02. The total dose rate consists of the contribution from the alpha, beta and gamma radiations as well as the contribution from the cosmic radiation.

Sample code	Depth (cm)	Grain size (µm)	Water content (% dry mass)	De (Gy)	U-Ra (Bq/kg)	Th (Bq/kg)	K (Bq/kg)	Total random error (%)	Total systematic error (%)	Total dose rate (Gy/ka)	Age (ka)	Weighted ages (ka)
END 1.1	77	4-11	1.1	3.1 ± 0.1 (n=13)	43.8±1.1	44.4±1.3	613±16	3.5	7.6	4.60 ± 0.07	0.7 ± 0.1	0.6 ± 0.0
		63-90		2.3 ± 0.0 (n=10)				2.6	5.4	3.87 ± 0.06	0.6 ± 0.0	
		90-125		2.3 ± 0.2 (n=10)				8.8	5.4	3.83 ± 0.06	0.6 ± 0.1	
END 1.2	147	4-11	1.7	10.1 ± 0.6 (n=10)	40.2±1.5	39.8±1.2	622±18	6.2	7.4	4.37 ± 0.07	2.3 ± 0.2	2.2 ± 0.1
		63-90		8.2 ± 0.2 (n=10)				3.0	5.4	3.70 ± 0.07	2.2 ± 0.1	
		90-125		7.8 ± 0.2 (n=11)				3.1	5.4	3.65 ± 0.06	2.1 ± 0.1	
END 1.3	207	4-11	2.2	10.7 ± 0.3 (n=11)	38.5±1.7	39.6±1.2	646±16	3.2	7.3	4.36 ± 0.07	2.5 ± 0.2	2.4 ± 0.1
		63-90		8.9 ± 0.1 (n=10)				2.0	5.5	3.70 ± 0.06	2.4 ± 0.1	
		90-125		8.9 ± 0.3 (n=10)				2.0	5.4	3.66 ± 0.06	2.4 ± 0.1	
END 1.4	307	4-11	2.7	14.6 ± 0.3 (n=10)	41.5±1.2	41.6±0.5	715±18	2.5	7.2	4.68 ± 0.06	3.1 ± 0.2	3.1 ± 0.2
		63-90		12.1 ± 0.2 (n=10)				2.2	5.5	3.98 ± 0.06	3.0 ± 0.2	
		90-125		12.2 ± 0.4 (n=11)				3.6	5.5	3.92 ± 0.06	3.1 ± 0.2	
END 1.5	398	4-11	4.2	29.0 ± 0.7 (n=13)	44.8±1.5	41.2±1.2	656±17	2.9	7.6	4.46 ± 0.07	6.5 ± 0.5	6.2 ± 0.4
		63-90		25.0 ± 1.1 (n=10)				4.7	5.6	3.77 ± 0.06	6.6 ± 0.5	
		90-125		22.0 ± 0.6 (n=10)				3.2	5.6	3.72 ± 0.06	5.9 ± 0.4	
END 1.6	455	4-11	3.9	29.6 ± 0.3 (n=10)	40.9±1.5	39.9±1.2	634±19	2.0	7.5	4.26 ± 0.08	6.9 ± 0.5	6.8 ± 0.4
		63-90		30.6 ± 1.1 (n=10)				4.0	5.6	3.61 ± 0.07	8.5 ± 0.6	
		90-125		23.8 ± 0.8 (n=10)				3.8	5.6	3.56 ± 0.07	6.7 ± 0.5	
END 1.7	506	4-11	5.4	43.4 ± 0.8 (n=12)	40.0±0.9	44.4±0.7	658±17	2.3	7.6	4.34 ± 0.06	10.0 ± 0.8	9.5 ± 0.6
		63-90		33.5 ± 0.7 (n=20)				2.6	5.7	3.67 ± 0.05	9.1 ± 0.6	
		90-125		35.7 ± 1.3 (n=10)				3.9	5.7	3.63 ± 0.05	9.8 ± 0.7	
END 1.8	546	4-11	6.7	47.3 ± 0.8(n=10)	44.2±1.8	43.9±1.2	627±18	2.4	7.9	4.27 ± 0.07	11.1 ± 0.9	11.5 ± 0.8
		63-90		42.3 ± 0.5 (n=58)				2.1	5.8	3.60 ± 0.06	11.8 ± 0.7	
		90-125		-				-	-	-	-	

Sample code	Depth (cm)	Grain size (µm)	Water content (% dry mass)	De (Gy)	U-Ra (Bq/kg)	Th (Bq/kg)	K (Bq/kg)	Total random error (%)	Total systematic error (%)	Total dose rate (Gy/ka)	Age (ka)	Weighted ages (ka)
END 1.9	564	4-11	7.3	57.4 ± 0.3 (n=11)	46.2±0.3	42.1±0.5	653±20	1.5	7.9	4.33 ± 0.06	13.2 ± 1.1	12.9 ± 0.8
		63-90		45.4 ± 0.8 (n=10)				2.4	5.9	3.66 ± 0.06	12.4 ± 0.8	
		90-125		47.5 ± 0.4 (n=10)				1.8	5.8	3.61 ± 0.06	13.2 ± 0.8	
END 1.10	579	4-11	4.9	58.0 ± 0.3 (n=11)	54.3±0.4	48.1±1.5	634±20	1.6	8.1	4.74 ± 0.07	12.2 ± 1.0	12.7 ± 0.8
		63-90		49.3 ± 0.9 (n=10)				2.5	5.6	3.95 ± 0.07	12.5 ± 0.8	
		90-125		52.0 ± 0.9 (n=11)				2.4	5.6	3.90 ± 0.07	13.3 ± 0.8	
END 1.11	601	4-11	2.0	51.8 ± 0.6 (n=11)	42.0±1.9	43.9±0.6	606±19	2.1	7.7	4.37 ± 0.08	11.9 ± 0.9	13.1 ± 0.8
		63-90		49.9 ± 1.1 (n=10)				2.9	5.5	3.67 ± 0.07	13.6 ± 0.8	
		90-125		49.0 ± 0.9 (n=10)				2.6	5.5	3.62 ± 0.07	13.5 ± 0.8	
END 1.12	649	4-11	4.7	60.0 ± 0.6 (n=10)	43.8±0.8	44.4±0.9	661±21	1.9	7.7	4.47 ± 0.07	13.4 ± 1.1	14.0 ± 0.9
		63-90		55.1 ± 2.3 (n=10)				4.5	5.6	3.77 ± 0.07	14.6 ± 1.1	
		90-125		52.4 ± 0.9 (n=11)				2.5	5.6	3.72 ± 0.07	14.1 ± 0.9	

Table 5.2. Summary of the luminescence and dosimetry data obtained for Kuma section. Weighted OSL ages are calculated according to Aitken (1985). The uncertainties associated with the luminescence and dosimetry data are random; the uncertainties mentioned with the optical ages are the overall uncertainties. All uncertainties represent 1σ. The ages were determined considering the "as found" water content, with a relative error of 25%; n denotes the number of accepted aliquots; beta attenuation and etching factor used for 63-90 µm and 90-125 µm fractions are 0.94±0.050 and 0.92±0.050, respectively; adopted alpha efficiency factor was 0.04±0.02. The total dose rate consists of the contribution from the alpha, beta and gamma radiations as well as the contribution from the cosmic radiation.

Sample code	Depth (cm)	Grain size (µm)	Water content (% dry mass)	De (Gy)	U-Ra (Bq/kg)	Th (Bq/kg)	K (Bq/kg)	Total random error (%)	Total systematic error (%)	Total dose rate (Gy/ka)	Age (ka)	Weighted ages (ka)
KUM 1.1	24	4-11	6.4	37.0 ± 0.4 (n=10)	44.7 ± 1.1	48.3 ± 2.6	647 ± 19	2.2	7.7	4.61 ± 0.09	8.0 ± 0.6	7.9 ± 0.5
		63-90		30.6 ± 0.6 (n=20)				2.7	5.6	3.89 ± 0.07	7.9 ± 0.5	
		90-125		29.9 ± 1.0 (n=10)				3.8	5.6	3.85 ± 0.07	7.8 ± 0.5	
KUM 1.2	37	4-11	5.4	47.2 ± 0.4 (n=10)	45.7 ± 2.3	43.9 ± 2.8	640 ± 19	2.3	7.6	4.54 ± 0.10	10.4 ± 0.8	10.5 ± 0.7
		63-90		42.4 ± 0.8 (n=20)				2.8	5.6	3.83 ± 0.08	11.1 ± 0.7	
		90-125		37.4 ± 1.4 (n=10)				4.3	5.6	3.79 ± 0.08	9.9 ± 0.7	

Sample code	Depth (cm)	Grain size (µm)	Water content (% dry mass)	De (Gy)	U-Ra (Bq/kg)	Th (Bq/kg)	K (Bq/kg)	Total random error (%)	Total systematic error (%)	Total dose rate (Gy/ka)	Age (ka)	Weighted ages (ka)
KUM 1.3	**53**	**4-11**	**2.5**	**51.3 ± 0.7 (n=10)**	**41.3 ± 2**	**42.9 ± 2.4**	**603 ± 21**	**2.6**	**7.5**	**4.41 ± 0.10**	**11.6 ± 0.9**	**12.4 ± 0.8**
		63-90		**48.8 ± 0.7 (n=20)**				**2.7**	**5.4**	**3.72 ± 0.09**	**13.1 ± 0.8**	
		90-125		**45.0 ± 1.1 (n=10)**				**3.3**	**5.4**	**3.67 ± 0.08**	**12.3 ± 0.8**	
KUM 1.4	**60**	**4-11**	**5.4**	**53.3 ± 1.1 (n=10)**	**42.4 ± 2.9**	**41.4 ± 1.8**	**607 ± 18**	**3.0**	**7.6**	**4.41 ± 0.09**	**12.5 ± 1.0**	**13.5 ± 0.9**
		63-90		**52.4 ± 0.8 (n=22)**				**2.6**	**5.6**	**3.61 ± 0.08**	**14.5 ± 0.9**	
		90-125		**47.1 ± 1.5 (n=10)**				**3.8**	**5.6**	**3.57 ± 0.07**	**13.2 ± 0.9**	
KUM 1.5	**67**	**4-11**	**5.0**	**58.1 ± 0.6 (n=10)**	**42.4 ± 2.5**	**44.8 ± 1.1**	**623 ± 16**	**2.0**	**7.6**	**4.41 ± 0.08**	**13.2 ± 1.0**	**14.0 ± 0.9**
		63-90		**52.4 ± 0.9 (n=19)**				**2.4**	**5.6**	**3.73 ± 0.06**	**14.1 ± 0.9**	
		90-125		**53.0 ± 1.1 (n=10)**				**2.7**	**5.5**	**3.68 ± 0.06**	**14.4 ± 0.9**	
KUM 1.6	**76**	**4-11**	**5.1**	**57.6 ± 0.5 (n=10)**	**43.9 ± 2.7**	**43.2 ± 1.2**	**603 ± 17**	**2.1**	**7.7**	**4.34 ± 0.08**	**13.3 ± 1.1**	**13.9 ± 0.9**
		63-90		**52.6 ± 0.8 (n=20)**				**2.4**	**5.6**	**3.65 ± 0.07**	**14.4 ± 0.9**	
		90-125		**49.6 ± 0.8 (n=10)**				**2.5**	**5.5**	**3.61 ± 0.07**	**13.7 ± 0.8**	
KUM 1.7	**102**	**4-11**	**4.1**	**42.1 ± 0.8 (n=10)**	**48.6 ± 1.5**	**43.2 ± 0.5**	**637 ± 16**	**2.3**	**7.7**	**4.62 ± 0.06**	**9.1 ± 0.7**	**13.1 ± 0.8**
		63-90		**53.8 ± 1.2 (n=19)**				**2.7**	**5.5**	**3.88 ± 0.06**	**13.9 ± 0.8**	
		90-125		**47.0 ± 1.9 (n=10)**				**4.3**	**5.5**	**3.83 ± 0.06**	**12.3 ± 0.9**	
KUM 1.8	**200**	**4-11**	**6.6**	**61.1 ± 1.2 (n=10)**	**43 ± 2.3**	**39.9 ± 0.5**	**672 ± 19**	**2.6**	**7.5**	**4.36 ± 0.08**	**14.0 ± 1.1**	**14.7 ± 0.9**
		63-90		**55.8 ± 1.1 (n=17)**				**2.7**	**5.7**	**3.71 ± 0.07**	**15.1 ± 1.0**	
		90-125		**53.6 ± 1.2 (n=10)**				**2.9**	**5.7**	**3.66 ± 0.07**	**14.7 ± 0.9**	

In order to evaluate the effect of a varying moisture content during burial on the luminescence ages we have calculated the ages using "as found" as well as averaged moisture contents of 5±1.3 % and 10±2.5 % for all samples at Enders and Kuma sections. The OSL ages display an increase with greater water content by about 5% and still agree within error limits.

5.5. Discussion

5.5.1. Implications for high-resolution paleoclimatic records from the Brady Soil and Bignell Loess at Enders and Wauneta sections

The new OSL chronology and other data obtained at Enders section provide important new support for interpretation of Great Plains loess as a high-resolution paleoclimatic record, especially for the Pleistocene-Holocene transition and the Holocene.

The application of typical intrinsic rigor tests of the OSL dating method as well as the use of three grain size fractions of quartz leads to high confidence in the OSL ages obtained from the Enders section. Furthermore, the new OSL dating results (**Figure 5.1, Table 5.1**) are largely consistent with earlier OSL and ^{14}C dating in similar stratigraphic positions at Wauneta and other sites. The weighted average ages of the two samples in upper Peoria Loess just below the Brady Soil Bkb horizon are 14.0±0.9 ka (649 cm) and 13.1±0.8 ka (601 cm), consistent with other results from the central Great Plains (Roberts et al., 2003; Mason et al., 2008). The weighted OSL ages obtained from the lowermost Brady Soil Bkb horizon and from just above the Brady Soil Akb horizon are 12.7±0.8 ka and 9.5±0.6 ka, respectively, in agreement with the previously published OSL and ^{14}C chronologies (Johnson and Willey, 2000; Mason et al., 2008; Miao et al., 2005; 2007a).

At Enders the age of 3.1±0.2 ka (307 cm) obtained in loess is younger than ages of 4.0-3.7 ka at the same stratigraphic position elsewhere, but the ages of 2.4±0.2 ka (207 cm) and 2.2±0.2 ka (147 cm) obtained in loess are close to stratigraphically equivalent ages of 2.6-2.3 ka elsewhere (Miao et al., 2007b). The age of 0.6±0.0 ka (77 cm) from the light-colored loess above the upper Holocene paleosol at Enders is consistent with ages from this stratigraphic interval at other sites (Miao et al., 2007b).

The Brady Soil is marked by finer grain size at both Enders and Wauneta sites, as are the two most distinct Holocene paleosols, at least in terms of the <16 μm fraction. Importantly, however, the fine-grained particle content is not uniformly high in the Brady Soil. We interpret the variation in fine-grained content as the result of significant changes in the conditions affecting the emission, transport, and/or deposition of dust (Újvári et al., 2016) during the period of Brady Soil formation. Changes in the wind speed distribution are one obvious explanation; another possibility is a shift toward lower dust emission from closer to more distant parts of the primary source area, increasing the relative contribution of finer dust from more distant sources. An intriguing alternative is that the fine-grained peaks correspond to changes in precipitation, affecting the proportions of wet and dry deposition. The OSL chronology at Enders does not allow definite assignment of the fine-grained peaks to more widely recognized stages of the last deglaciation. The deepest peak could fall just before or in the early part of the Younger Dryas (Alley et al., 1993; Alley, 2000) and the upper two apparently fall after the end of the Younger Dryas.

Comparison of the magnetic measurements at the Enders and Wauneta sites suggests that these properties are influenced by both regional climatic change and local effects.

The greatest difference between the Enders and Wauneta sections is in the relative thickness of the relatively unweathered loess between the Brady Soil and the lower prominent Holocene soil.

5.5.2. Contrast with Eurasian loess records of the last glacial-interglacial transition and Holocene

The new chronology presented for Enders section supports earlier interpretations that the most significant Late Pleistocene to Holocene interval of soil formation, producing the Brady Soil (12.7±0.8 - 9.5±0.6 ka), spanned the Pleistocene-Holocene boundary.

On the other hand, at Kuma section the modern soil merges probably several paleosols, including the Brady soil and the Holocene Bignell loess is absent. We place the threshold in the magnetic susceptibility variation at 50 cm and we interpret it as likely reflecting the onset of soil formation during the Pleistocene to Holocene transition. An OSL weighted average age of 12.4±0.8 ka (53 cm) has been obtained at almost the same depth with χ_{lf} threshold. The OSL ages show that the onset of magnetic susceptibility enhancement at Kuma precedes the accepted stratigraphic Pleistocene-Holocene boundary dated at 11.7 ka in ice core records (Rasmussen et al., 2014). The weighted average ages of the two samples collected from Peoria Loess are 14.7±0.9 ka (200 cm) and 13.1±0.8 ka (102 cm), consistent with ages obtained at Enders section as well as with other results from the central Great Plains (Roberts et al., 2003; Mason et al., 2008).

In Eurasian loess records, from the Danubian loess of southeastern Europe to the Chinese Loess Plateau, soil formation began later than in the central Great Plains and continued through all or much of the Holocene (Stevens et al., 2011; Dong et al., 2015; Marković et al., 2014; 2018; Constantin et al., 2019). In China, however, the Holocene soil S0 in some sections closer to dry source regions of the loess represents a complex sequence of loess accumulation and pedogenesis, relatively similar to the Brady Soil. Finally most Chinese S0 profiles are buried by latest Holocene loess (L0) (e.g. Baicaoyuan, Shiguanzhi, Yuanbaosections) (Lai and Wintle, 2006; Stevens et al., 2006; Zhao et al., 2013).

5.6. Conclusions

Optically stimulated luminescence dating of 4-11 µm, 63-90 µm and 90-125 µm quartz has been reported for the Enders and Kuma sections located in southwestern Nebraska, midcontinental North America. The Enders section includes well-preserved Peoria Loess, Brady Soil and Bignell Loess units. At Kuma section, Peoria loess is capped by modern soil, which merges probably several paleosols, including the Brady soil and the Bignell loess is not apparent. Based on the successful results of typical intrinsic rigor tests of the SAR protocol and agreement between the three grain size fractions of quartz, we are fully confident that the obtained OSL ages are accurate. By averaging the three sets of ages available for each sample, the overall error has been reduced to around 4-6%, demonstrating the potential of improving the precision of luminescence dating.

Here we have shown that with adequate age control and high-resolution sampling, loess sections in the central Great Plains can provide a regionally coherent record of the Pleistocene-Holocene transition and Holocene climatic change, not just at the orbital to millennial-scale resolution of visible paleosols and loess units but at a finer millennial to centennial timescale. That goal is important not only for understanding the paleoclimatic history of the Great Plains region, but also for comparison with the loess record of Eurasia.

Conclusions

Loess-palaeosol sequences are continental archives of Quaternary paleoclimates and loess can be dated directly using luminescence dating. Due to environmental differences between loess records from different continents, it is essential to establish proper chronologies of loess deposits. Luminescence methods (IRSL and OSL) represent one of the most valuable chronological tools available for Quaternary studies. A robust luminescence dating coupled with multi-proxy analysis (e.g. grain size, magnetic susceptibility, geochemical data) can provide a high-resolution paleoclimatic record from loess-paleosol sequences.

The OSL investigations of Kurortne LPS (Ukraine), obtained on quartz grains of different grain sizes (4-11 µm, 63-90 µm and 90-125µm), confirm the previous findings obtained on loess-paleosol sequences located on the Black Sea shore in Romania as well as worldwide: (i) ages obtained on different grain sizes are in agreement for equivalent doses of less than 200 Gy, whereas for higher equivalent doses 4-11 µm ages underestimate the coarser fraction ages; and (ii) an inverse correlation between dated grain size and saturation characteristics is reported. As the temporal range covered by Kaydaky-Pryluky paleosol units in the Ukrainian Quaternary stratigraphic framework is still debatable, our results confirm the broad correlation of those units at Kurortne with the last interglacial (i.e., MIS 5). Dating the Uday and Bug loess units produced ages corresponding to MIS 4 and MIS 2, respectively, whereas the sample collected from the Vytachiv unit provided an age of 37.7 ± 2.4 ka, assigning this paleosol to MIS 3. On the basis of trends in the magnetic enhancement, the onset of pedogenetic processes likely commenced already around 20 ka, but the formation of the topmost S0 soil has begun after 13.8 ± 1.0 ka. The results based on integrating luminescence dating with multi-proxy sedimentological data for Kurortne LPS clarify local chronostratigraphic correlations, establish more secure reconstructions of Late Pleistocene environmental changes in the northern Black Sea area.

The robust luminescence chronology for Stayky LPS (Ukraine), based on OSL dating on quartz (4-11 µm, 63-90 µm) and post infrared-infrared stimulated luminescence (pIR-IRSL) on polymineral fine grains, demonstrated that the results obtained for the Bug loess (the equivalent of MIS 2) are in agreement between methods. The study indicated that the suite of embryonic soils previously interpreted as reflecting climate variability similar to Greenland interstadials (GI) actually date to ~29/27-15 ka, with most emplaced around or after 20 ka. Apart from GI-2, no interstadial-type climate events are recorded in Greenland ice core data for that time interval. The dating of Vytachiv paleosol, previously debatably linked to various interstadial events within MIS 3 indicate that it developed during middle-to-late MIS 3. The dating of Pryluky unit indicated that the pIR-$IRSL_{290}$ data confirm the broad correspondence of this unit with MIS 5, while quartz results severely underestimate these ages. For Dnieper till unit, no reliable OSL ages have been obtained because the signals emitted by polymineral fine grains and quartz were found in saturation and close to saturation, respectively. This study suggested that the Stayky LPS record could be considered as a reference site in mid-latitude European loess paleoclimatology at least for MIS 2, clarifying several previously un-resolved chronostratigraphic issues.

The first OSL investigations of Enders and Kuma sections (Nebraska, North America), obtained on quartz grains of different grain sizes (4-11 µm, 63-90 µm and 90-125 µm), indicated that Peoria Loess deposition ended around 13-14 ka at both sections. At Enders section, the termination of Peoria Loess deposition is marked by the Brady Soil, bracketed by OSL ages of 12.7 ± 0.8 ka to 9.5 ± 0.6 ka and the Bignell Loess accumulated episodically throughout the Holocene, starting from around 9.5 ka. The new chronology presented for Enders section supports earlier interpretations that the most significant Late Pleistocene to Holocene interval of soil formation, producing the Brady Soil, spanned the Pleistocene-Holocene boundary. By averaging the three sets of ages obtained for each sample, the overall error has been reduced to around 4-6%, demonstrating the potential of improving the precision of luminescence dating. Based on the threshold of the magnetic signal enhancement the beginning of the modern soil formation has been placed at around 12.4 ± 0.8 ka at Kuma site. Thus, the onset of the magnetic signal enhancement produced by pedogenesis in the Kuma site started before the stratigraphic Pleistocene-Holocene transition dated at 11.7 ka in ice core records.

This thesis demonstrated that a robust luminescence chronology coupled with multi-proxy analysis (i.e. grain size, magnetic susceptibility, and geochemical data) obtained on European and North American loess-palaeosol sequences provide a regionally coherent record of the Late Pleistocene-Holocene climate changes.

References

Aitken, M.J., and Alldred, J.C., 1972. The assessment of error limits in thermoluminescent dating. Archaeometry 14, 257-267.

Aitken, M.J., 1976. Thermoluminescent age evaluation and assessment of error limits: revised system. Archaeometry 18, 233-238.

Aitken, M.J., 1985. Thermoluminescence dating. Academic press, London, 359 p.

Aitken, M.J., 1998. An introduction to optical dating. Oxford: Oxford University Press, 280 p.

Alley, R.B., Meese, D.A., Shuman, C.A., Gow, A.J., Taylor, K.C., Grootes, P.M., White, J.W.C., Ram, M., Waddington, E.D., Mayewski, P.A., Zielinski, G.A., 1993. Abrupt increase in Greenland snow accumulation at the end of the Younger Dryas event. Nature 362, 527-529.

Alley, R.B., and Clark, P.U., 1999. The deglaciation of the northern hemisphere: a global perspective. Annual Reviews of Earth and Planetary Sciences 27, 149-182.

Alley, R.B., 2000. The Younger Dryas cold interval as viewed from central Greenland. Quaternary Science Reviews 19, 213-226.

Antoine, P., Rousseau, D.D., Zöller, L., Lang, A., Munaut, A.V., Hatté , C., Fontugne, M., 2001. High resolution record of the last interglacial–glacial cycle in the Nussloch loess–palaeosol sequences, Upper Rhine Area Germany. Quaternary International 76–77, 211-229.

Antoine, P., Rousseau, D.-D., Moine, O., Kunesch, S., Hatté, C., Lang, A., Tissoux, H., Zöller, L., 2009. Rapid and cyclic Aeolian deposition during the Last Glacial in European loess: a high resolution record from Nussloch, Germany, Quaternary Science Reviews 28, 2955-2973.

Antoine, P., Rousseau, D.-D., Degeai, J.-P., Moine, O., Lagroix, F., Kreutzer, S., Fuchs, M., Hatté, C., Gauthier, C., Svoboda, J., Lisá, L., 2013. High-resolution record of the environmental response to climatic variations during the Last Interglaciale Glacial cycle in Central Europe: the loess-palaeosol sequence of Dolní Vestonice (Czech Republic), Quaternary Science Reviews 67, 17-38.

Basarin, B., Buggle, B., Hambach, U., Marković, S.B., Dhand, K.O., Kovačević, A., Stevens, T., Guo, Z., Lukić, T., 2014. Time-scale and astronomical forcing of Serbian loess–paleosolsequences. Global and Planetary Change 122, 89-106.

Bokhorst, M., Vandenberge, J., Sumegi, P., Lanzont M., Gerasimenko, N., Matviishina, Zh., Markovich, S., Frechen, M., 2011. Atmospheric circulation patterns in central and eastern Europe during the Weichselian pleniglacial inferred from loess grain-size record. Quaternary International 1-2, 62-74.

Bond, G.C., Broecker, W., Johnsen, S., McManus, J., Labeyrie, L., Jouzel, J., Bonani, G., 1993. Correlations between climate records from North Atlantic sediments and Greenland ice. Nature 365, 143-147.

Buggle, B., Glaser, B., Zöller, L., Hambach, U., Marković, S., Glaser, I., Gerasimenko, N., 2008. Geochemical characterization and origin of Southeastern and Eastern European loesses (Serbia, Romania, Ukraine). Quaternary Science Reviews 27, 1058-1075.

Buggle, B., Hambach, U., Glaser, B., Gerasimenko, N., Marković, S., Glaser, I., Zöller, L., 2009. Stratigraphy, and spatial and temporal paleoclimatic trends in Southeastern/Eastern European loess–paleosol sequences. Quaternary International 196, 86-106.

Buylaert, J.P., Huot, S., Murray, A.S., Van den haute, P., 2011. Infrared stimulated luminescence dating of an Eemian (MIS 5e) site in Denmark using K-feldspar. Boreas 40, 46-56.

Buylaert, J.P., Jain, M., Murray, A.S., Thomsen, K.J., Thiel, C., Sohbati, R., 2012. A robust feldspar luminescence dating method for Middle and Late Pleistocene sediments. Boreas 41, 435-451.

Constantin, D., Begy, R., Vasiliniuc, S., Panaiotu, C., Necula, C., Codrea, V., Timar-Gabor, A., 2014. High resolution OSL dating of the Costinești section Romania using fine and coarse quartz. Quaternary International 334-335, 20-29.

Constantin, D., Camenita, A., Panaiotu, C., Necula, C., Codrea, V., Timar-Gabor, A., 2015. Fine and coarse-quartz SAR-OSL dating of Last Glacial loess in Southern Romania. Quaternary International 357, 33-43.

Constantin, D., Veres, D., Panaiotu, C., Anechitei-Deacu, V., Groza, S.M., Begy, R., Kelemen, S., Buylaert, J.-P., Hambach, U., Marković, S.B., Gerasimenko, N., Timar-Gabor, A. 2019. Luminescence age constraints on the Pleistocene-Holocene transition recorded in loess sequences across SE Europe. Quaternary Geochronology 49, 71-77.

Dansgaard, W., Johnsen, S., Clausen, H.B., Dahl-Jensen, D., Gundestrup, N., Hammer, C.U., Oeschger, H., 1984. North Atlantic climatic oscillations revealed by deep Greenland ice cores. In: Hansen, J.E., Takahashi, T. (Eds.), Climate Processes and Climate Sensitivity. American Geophysical Union, Washington DC, 288-298.

Dansgaard, W., Johnsen, S.J., Clausen, H.B., Dahl-Jensen, D., Gundestrup, N.S., Hammer, C.U., Hvidberg, C.S., Steffensen, J.P., Sveinbjörnsdottir, A.E., Jouzel, J., Bond, G., 1993. Evidence for general instability of past climate from a 250-kyr ice-core record. Nature 364, 218–220.

Dearing, J.A., Dann, R.J.L., Hay, K., Lees, J.A., Loveland, P.J., Maher, B.A., O'Grady, K., 1996. Frequency-dependent susceptibility measurements of environmental materials. Geophysical Journal International 124, 228-240.

Dong, Y., Wu, N., Li, F., Huang, L., Wen, W., 2015. Time-transgressive nature of the magnetic susceptibility record across the Chinese Loess Plateau at the Pleistocene/ Holocene transition. PLoS One 10, e0133541.

Duller, G.A.T., 2003. Distinguishing quartz and feldspar in single grain luminescence measurements. Radiation Measurements 37, 161-165.

Fu, X., and Li, S-H., 2013. A modified multi-elevated-temperature post IR-IRSL protocol for dating Holocence sediments using K-feldspar. Quaternary Geochronology 17, 44-54.

Fuchs, M., Kreutzer, S., Rousseau, D.D., Antoine, P., Hatté, C., Lagroix, F., Moine, O., Gauthier, C., Svoboda, J., Lisá, L., 2012. The loess sequence of Dolní Věstonice (Czech Republic): a new OSL based chronology of the Last Climatic Cycle. Boreas 42, 664-677.

Gerasimenko, N.P., 2004. Rozvytok zonal'nyh landshaftiv chetvertynnogo periodu v Ukraina (Quaternary evolution of zonal paleoecosystems in Ukraine). Geographical Institute of National Ukrainian Academy of Sciences, Kyiv (in Ukrainian).

Gerasimenko, N., 2006. Upper Pleistocene loess-palaeosol and vegetational successions in the Middle Dnieper Area, Ukraine. Quaternary International 149, 55-66.

Gerasimenko, N., and Rousseau, D.-D., 2008. Stratigraphy and paleoenvironments of the Last Pleniglacial in the Kyiv loess region (Ukraine). Quaternaire 19, 293-307.

Gerasimenko, N., 2011. Climatic and environmental oscillations in southeastern Ukraine from 30 to 10 ka, inferred from pollen and lithopedology. Geology and geoarchaeology of the Black Sea region: beyond the Flood hypothesis. Geological Society of America Special Papers 473, 117-132.

Gozhik, P.F., Shelkoplyas, V.M., Komar, M.S., Matviishina, Zh.M., Perederiy, V.I., 2000. Putivnyk X Pol'sko-Ukrainskogo seminaru „Koreluatsia lesiv i lyodovykovyh vidkladiv Pol'shchi ta Ukrainy (Excursion Guide of Xth Polish-Ukrainian Seminar "Correlation of loesses and glacial deposits of Poland and Ukraine"). Institute of Geological Sciences, Kyiv.

Gozhik, P., Matviishina, Zh., Shelkoplyas, V., Palienko, V., Rekovets, L., Gerasimenko, N., Korniets, N., 2001. The Upper and Middle Pleistocene of Ukraine. In: The Ukraine Quaternary Explored: The Middle and Upper Pleistocene of the Middle Dnieper Area and its Importance for the East-West Correlation, Volume of Abstracts. IGS NASU, Kyiv, 32-34.

Gozhik, P., Komar, M., Lanćzont, M., Fedorovicz, S., Bogucki, A., Mroczek, P., Prylypko, S., Kusiak, J., 2014. Paleoenvironmental history of the Middle Dnieper Area from the Dnieper to Weichselian Glaciation: a case study of the Maxymivka loess profile. Quaternary International 334-335, 94-111.

Grootes, P.M., Stuiver, M., White, W.C., Johnsen, S., Jouzel, J., 1993. Comparison of oxygen isotope records from the GISP2 and GRIP Greenland Ice cores. Nature 366, 552–554.

Guérin, G., Mercier, N., Adamiec, G., 2011. Dose-rate conversion factors: update. Ancient TL, 29, 5-8.

Haase, D., Fink, J., Haase, G., Ruske, R., Pécsi, M., Richter, H., Altermann, M., Jäger, K-D., 2007. Loess in Europe - its spatial distribution based on a European Loess Map, 1:2500000. Quaternary Science Reviews 26, 1301-1312.

Heinrich, H., 1988. Origin and consequences of cyclic ice rafting in the northeast Atlantic ocean during the past 130,000 years. Quaternary Research 29, 142-152.

Huntley, D.J., Godfrey-Smith, D.I., Thewalt, M.L.W., 1985. Optical dating of sediments. Nature 313, 105-107.

Huntley, D.J., and Lamothe, M., 2001. Ubiquity of anomalous fading in K-feldspars and the measurement and correction for it in optical dating. Canadian Journal of Earth Sciences 38, 1093-1106.

ISO 13320, 2009. Particle size analysis - Laser diffraction methods. International Organization for Standardization, Geneva.

Johnson, W.C., and Willey, K.L., 2000. Isotopic and rock magnetic expression of environmental change at the Pleistocene-Holocene transition in the central Great Plains. Quaternary International 67, 89-106.

Jordanova, D., and Petersen, N., 1999. Palaeoclimatic record from a loess-soil profile in northeastern Bulgaria-II. Correlation with global climatic events during the Pleistocene. Geophysical Journal International 138, 533-540.

Kadereit, A., and Wagner, G., 2014. Geochronological reconsideration of the eastern European key loess section at Stayky in Ukraine. Climate of the Past 10, 783-796.

Krupskyi, N.K., and Polupan, N.I., 1979. Atlat pochv Ukrainskoy SSR (Soil Atlas of the Ukrainian SSR). Urozhay, Kiev (in Ukrainian).

Kuzila, M.S., 1995. Identification of multiple loess units within modern soils of Clay County. Nebraska. Geoderma 65, 45-47.

Lai, Z.P., and Wintle, A.G., 2006. Locating the boundary between the Pleistocene and the Holocene in Chinese loess using luminescence. The Holocene 16, 893-99.

Lapp, T., Kook, M., Murray, A.S., Thomsen, K.J., Buylaert, J.-P., Jain, M., 2015. A new luminescence Detection and Stimulation Head for the Risø TL/OSL reader. Radiation Measurement 81, 178-184.

Li, B., and Li, S.H., 2011. Luminescence dating of K-feldspar from sediments: A protocol without anomalous fading correction. Quaternary Geochronology 6, 468-479.

Lisiecki, L.E., and Raymo, M.E., 2005. A Pliocene-Pleistocene stack of 57 globally distributed benthic $\delta^{18}O$ records. Paleoceanography 20, PA1003.

Maher, B.A., Thompson, R., Zhou, L.P., 1994. Spatial and temporal reconstructions of changes in the Asian palaeomonsoon: a new mineral magnetic approach. Earth and Planetary Science Letters 125, 461-471.

Marković, S.B., Timar-Gabor, A., Stevens, T., Hambach, U., Popov, D., Tomić, N., Obreht, I., Jovanović, M., Lehmkuhl, F., Kels, H., Marković, R., Gavrilov, M.B., 2014. Environmental dynamics and luminescence chronology from the Orlovat loess–palaeosol sequence (Vojvodina, northern Serbia). Journal of Quaternary Science 29, 189-199.

Marković, S.B., Stevens, T., Kukla, G.J., Hambach, U., Fitzsimmons, K.E., Gibbard, P., Buggle, B., Zech, M., Guo, Z., Hao, Q., Wu, H., O'Hara Dhand, K., Smalley, I.J., Újvári, G., Sümegi, P., Timar-Gabor, A., Veres, D., Sirocko, F., Vasiljević, D.A., Jary, Z., Svensson, A., Jović, V., Lehmkuhl, F., Kovács, J., Svirčev, Z., 2015. Danube loess stratigraphy - Towards a pan-European loess stratigraphic model. Earth-Science Reviews 148, 228-258.

Marković, S.B., Stevens, T., Vandenberghe, J., Veres, D., Újvári, G., Timar-Gabor, A., Zeeden, C., Guo, Z., Hao, Q., Obreht, I., Hambach, U., Wu, H., Gavrilov, M.B., Rolf, C., Tomić, N., Lehmkuhl, F., 2018. Loess correlations - between myth and reality. Palaeogeography, Palaeoclimatology, Palaeoecology 509, 4-23.

Mason, J.A., Miao, X.D., Hanson, P.R., Johnson, W.C., Jacobs, P.M., Goble, R. J., 2008. Loess record of the Pleistocene-Holocene transition on the northern and central Great Plains, USA. Quaternary Science Reviews 27, 1772-1783.

Mejdahl, V., 1979. Thermoluminescence dating: beta-dose attenuation in quartz grains. Archaeometry 21, 61-72.

Miao, X., Mason, J.A., Goble, R.J., Hanson, P.R., 2005. Loess record of dry climate and aeolian activity in the early-to mid-Holocene, central Great Plains, North America. The Holocene 15, 339-346.

Miao, X., Mason, J.A., Johnson, W.C., Wang, H., 2007a. High-resolution proxy record of Holocene climate from a loess section in Southwestern Nebraska, USA. Palaeogeography, Palaeoclimatology, Palaeoecology 245, 368-381.

Miao, X.D., Mason, J.A., Swinehart, J.B., Loope, D.B., Hanson, P.R., Goble, R.J., Liu, X.D., 2007b. A 10,000-yr record of dune activity, dust storms, and severe drought in the central Great Plains, U.S.A. Geology 35, 119-122.

Muhs, D.R., McGeehin, J.P., Beann, J., Fisher, E., 2004. Holocene loess deposition and soil formation as competing processes, Matanuska Valley, southern Alaska. Quaternary Research 61, 265-276.

Muhs, D.R., 2013. Loess and its Geomorphic, Stratigraphic, and Paleoclimatic Significance in the Quaternary, in: Treatise on Geomorphology. Academic Press, San Diego, 149-183.

Murray, A.S., and Wintle, A.G., 2000. Luminescence dating of quartz using an improved single-aliquot regenerative-dose protocol. Radiation Measurements 32, 57-73.

Murray, A.S. and Wintle, A.G., 2003. The single aliquot regenerative dose protocol: potential for improvements in reliability. Radiation Measurements 37, 377-381.

National Research Council, 2001. Abrupt Climate Change: Inevitable Surprises (National Academies Press).

Necula, C., Panaiotu, C., Heslop, D., Dimofte, D., 2013. Climatic control of magnetic granulometry in the Mircea Vodă loess/paleosol sequence (Dobrogea, Romania). Quaternary International 293, 5-14.

Necula, C., Dimofte, D., Panaiotu, C., 2015. Rock magnetism of a loess-palaeosol sequence from the western Black Sea shore (Romania). Geophysical Journal International 202 (3), 1733-1748.

Nesbitt, H.W., and Young, G.M., 1982. Early Proterozoic climates and plate motions inferred from major element chemistry of lutites. Nature 299, 715-717.

Obreht, I., Hambach, U., Veres, D., Zeeden, C., Bösken, J., Stevens, T., Marković, S.B., Klasen, N., Brill, D., Burow, C., Lehmkuhl, F., 2017. Shift of large-scale atmospheric systems over Europe during late MIS 3 and implications for Modern Human dispersal. Scientific Reports 7, 5848.

Özer, M., Orhan, M., Işik, N.S., 2010. Effect of Particle Optical Properties on Size Distribution of Soils Obtained by Laser Diffraction. Environmental & Engineering Geoscience 16, 163-173.

Porter, S.C., 2001. Chinese loess record of monsoon climate during the last glacial–interglacial cycle. Earth-Science Reviews 54, 115-128.

Porter, S.C., and An, Z.S., 1995. Correlation between climate events in the North Atlantic and China during the last glaciation. Nature 375, 305-308.

Prescott, J.R., Hutton, J.T., 1994. Cosmic ray contributions to dose rates for luminescence and ESR dating: Large depths and long term variations. Radiation Measurements 23, 497-500.

Pye, K., 1987. Aeolian Dust and Dust Deposits. San Diego, CA: Academic Press, 334 p.

Rasmussen, S.O., Bigler, M., Blockley, S.P., Blunier, T., Buchardt, S.L., Clausen, H.B., Cvijanovic, I., Dahl-Jensen, D., Johnsen, S.J., Fischer, H., Gkinis, V., Guillevic, M., Hoek, W.Z., Lowe, J.J., Pedro, J.B., Popp, T., Seierstad, I.K., Steffensen, J.P., Svensson, A.M., Vallelonga, P., Vinther, B.M., Walker, M.J.C., Wheatley, J.J., Winstrup, M., 2014. A stratigraphic framework for abrupt climatic changes during the Last Glacial period based on three synchronized Greenland ice-core records: refining and extending the INTIMATE event stratigraphy. Quaternary Science Reviews 106, 14-28.

Rees-Jones, J., 1995. Optical dating of young sediments using fine-grain quartz. Ancient TL 13, 9-13.

Roberts, H.M., Wintle, A.G., Maher, B.A., Hu, M., 2001. Holocene sediment-accumulation rates in the western Loess Plateau, China, and a 2500-year record of agricultural activity, revealed by OSL dating. The Holocene 11, 477–483.

Roberts, H.M., Muhs, D.R., Wintle, A.G., Duller, G.A.T., Bettis III, E.A., 2003. Unprecedented last glacial mass accumulation rates determined by luminescence dating of loess from western Nebraska. Quaternary Research 59, 411-419.

Rousseau, D.-D., Gerasimenko, N., Matviishina, Zh., Kukla, G., 2001. Late Pleistocene environments of Central Ukraine. Quaternary Research 56, 349-356.

Rousseau, D.-D., Antoine, P., Hatté, C., Lang, A., Zöller, L., Fontugne, M., Ben Othman, D., Luck, J.-M., Moine, O., Labonne, M., Bentaleb, I., Jolly, D., 2002. Abrupt millennial climatic changes from

Nussloch (Germany) Upper Weichselian eolian records during the last glaciation. Quaternary Science Reviews 21, 1577-1582.

Rousseau, D.-D., Sima, A., Antoine, P., Hatté, C., Lang, A., Zöller, L., 2007. Link between European and North-Atlantic abrupt climate changes over the last glaciation. Geophysical Research Letters 34, L22713.

Rousseau, D.-D., Antoine, P., Gerasimenko, N., Sima, A., Fuchs, M., Hatté, C., Moine, O., Zoeller, L., 2011. North Atlantic abrupt climatic events of the last glacial period recorded in Ukrainian loess deposits, Climate of the Past 7, 221-234.

Rousseau, D.-D., Boers, N., Sima, A., Svensson, A., Bigler, M., Lagroix, F., Taylor, S., Antoine, P., 2017b. (MIS3 & 2) millennial oscillations in Greenland dust and Eurasian aeolian records – A paleosol perspective. Quaternary Science Reviews 169, 99-113.

Ruth, U., Bigler, M., Röthlisberger, R., Siggaard-Andersen, M.-L., Kipfstuhl, S., Goto-Azuma, K., Hansson, M.E., Johnsen, S.J., Lu, H., Steffensen, J.P., 2007. Ice core evidence for a very tight link between North Atlantic and east Asian glacial climate. Geophysical Research Letters 34, L03706.

Schulte, P., Lehmkuhl, F., Steininger, F., Loibl, D., Lockot, G., Protze, J., Fischer, P., Stauch, G., 2016. Influence of HCl pretreatment and organo-mineral complexes on laser diffraction measurement of loess-paleosol-sequences. CATENA 137, 392-405.

Schulz, H., von Rad, U., Erlenkeuser, H., 1998. Correlation between Arabian Sea and Greenland climate oscillations of the past 110,000 years. Nature 393, 54–57.

Sima, A., Rousseau, D.-D., Kageyama, M., Ramstein, G., Schulz, M., Balkanski, Y., Antoine, P., Dulac, F., Hatté, C., 2009. Imprint of North-Atlantic abrupt climate changes on western European loess deposits as viewed in a dust emission model, Quaternary Science Reviews 28, 2851-2866.

Sima, A., Kageyama, M., Rousseau, D.D., Ramstein, P., Balkanski, Y., Antoine, P., Hatte, C., 2013. Modeling dust emission response to North Atlantic millennial- scale climate variations from the perspective of East European MIS 3 loess deposits. Climate of the Past 9, 1385-1402.

Singer, M.J., and Verosub, K.L., 2007. Mineral magnetic analysis. In: Elias, S. (Ed.). The Encyclopedia of Quaternary Sciences. Elsevier, Amsterdam, 2096-2102.

Sirenko, N.A., and Turlo S.I., 1986. Razvitie pochv i rastitel'nosti Ukrainy v pliotsene i pleistostene (Soil and vegetational development in Ukraine during the Pliocene and Pleistocene). Naukova Dumka, Kyiv (in Russian).

SPECTRO, 2007. Analysis of trace elements in geological materials, soils and sludges prepared as pressed pellets, Report XRF. SPECTRO.

Stevens, T., Armitage, S.J., Lu, H.Y., Thomas, D.S.G., 2006. Sedimentation and diagenesis of Chinese loess: implications for the preservation of continuous, high-resolution climate records. Geology 34, 849-852.

Stevens, T., Markovic, S.B., Zech, M., Hambach, U., Sümegi, P., 2011. Dust deposition and climate in the Carpathian Basin over an independently dated last glacial-interglacial cycle. Quaternary Science Reviews 30, 662-681.

Sun, Y.B., Clemens, S.C., Morrill, C., Lin, X.P., Wang, X.L., An, Z.S., 2012. Influence of Atlantic meridional overturning circulation on the East Asian winter monsoon. Nature Geoscience 5, 46-49.

Svensson, A., Andersen, K.K., Bigler, B., Clausen, H.B., Dahl-Jensen, D., Davies, S.M., Johnsen, S.J., Muscheler, R., Rasmussen, S.O., Röthlisberger, R., Steffensen, J.P., Vinther, B.M., 2006. The Greenland Ice Core Chronology 2005, 15–42 ka. Part 2: comparison to other records. Quaternary Science Reviews 25, 3258-3267.

Svensson, A., Andersen, K.K., Bigler, M., Clausen, H.B., Dahl-Jensen, D., Davies, S.M., Johnsen, S.J., Muscheler, R., Parrenin, F., Rasmussen, S.O., Roethlisberger, R., Seierstad, I., Steffensen, J.P., Vinther, B.M., 2008. A 60 000 year Greenland stratigraphic ice core chronology. Climate of the Past 4, 47-57.

Tecsa, V., Gerasimenko, N., Veres, D., Hambach, U., Lehmkuhl, F., Schulte, P., Timar-Gabor, A., 2020a. Revisiting the chronostratigraphy of Late Pleistocene loess-paleosol sequences in southwestern Ukraine: OSL dating of Kurortne section. Quaternary International 542, 65-79.

Tecsa, V., Mason, J.A., Johnson, W.C., Miao, X., Constantin, D., Radu, S., Magdas, D.A., Veres, D., Marković, S.B., Timar-Gabor, A., 2020b. Latest Pleistocene to Holocene loess in the central Great Plains: Optically stimulated luminescence dating and multi-proxy analysis of the Enders loess section (Nebraska, USA). Quaternary Science Reviews 229, 106130.

Thiel, C., Buylaert, J.P., Murray, A.S., Terhorst, B., Hofer, I., Tsukamoto, S., Frechen, M., 2011. Luminescence dating of the Stratzing loess profile (Austria) - testing the potential of an elevated temperature post-IR IRSL protocol. Quaternary International 234, 23-31.

Thomsen, K.J., Bøtter-Jensen, L., Denby, P.M., Moska, P., Murray, A.S., 2006. Developments in luminescence measurement techniques. Radiation Measurements 41, 768-773.

Timar, A., Vandenberghe, D., Panaiotu, C.G., Necula, C., Cosma, C., van den Haute, P., 2010. Optical dating of Romanian loess using fine-grained quartz. Quaternary Geochronology 5, 143-148.

Timar-Gabor, A., Vandenberghe, D.A.G., Vasiliniuc, S., Panaiotu, C.G., Dimofte, D., Cosma, C., 2011. Optical dating of Romanian loess: a comparison between silt-sized and sand-sized quartz. Quaternary International 240, 62-70.

Timar-Gabor, A., Vasiliniuc, S., Vandenberghe, D.A.G., Cosma, C., Wintle, A.G., 2012. Investigations into the reliability of SAR-OSL equivalent doses obtained for quartz samples displaying dose response curves with more than one component. Radion Measurements 47, 740-745.

Timar-Gabor, A., Constantin, D., Marković, S.B., Jain, M., 2015. Extending the area of investigation of fine versus coarse quartz optical ages from the Lower Danube to the Carpathian Basin. Quaternary International 388, 168-176.

Timar-Gabor, A., Buylaert, J.-P., Guralnik, B., Trandafir-Antohi, O., Constantin, D., Anechitei-Deacu, V., Jain, M., Murray, A.S., Porat, N., Hao, Q., Wintle, A.G., 2017. On the importance of grain size in luminescence dating using quartz. Radiation Measurements 106, 464-471.

Újvári, G., Kok, J.F., Varga, G., Kovács, J., 2016. The physics of wind-blown loess: Implications for grain size proxy interpretations in Quaternary paleoclimate studies. Earth-Science Reviews 154, 247-278.

Vandenberghe, J., Renssen, H., van Huissteden, K., Nugteren, G., Konert, M., Lu, H., Dodonov, A., Buylaert, J.-P., 2006. Penetration of Atlantic westerly winds into central and East Asia. Quaternary Science Reviews 25, 2380-2389.

Vandenberghe, D.A.G., De Corte, F., Buylaert, J.-P., Kučera, J., Van den haute, P., 2008. On the internal radioactivity in quartz. Radiation Measurements 43, 771-775.

Veres, D., Tecsa, V., Gerasimenko, N., Zeeden, C., Hambach, U., Timar-Gabor, A., 2018. Short-term soil formation events in last glacial East European loess, evidence from multi-method luminescence dating. Quaternary Science Review 200, 34–51.

Verosub, K.L., Fine, P., Singer, M.J., TenPas, J., 1993. Pedogenesis and paleoclimate: interpretation of the magnetic susceptibility record of Chinese loess–paleosol sequences. Geology 21, 1011-1014.

Wintle, A.G., 1973. Anomalous fading of thermoluminescence in mineral samples. Nature 245, 143-144.

Wintle, A.G., and Murray, A.S., 2006. A review of quartz optically stimulated luminescence characteristics and their relevance in single-aliquot regeneration dating protocols. Radiation Measurements 41, 369-391.

Zeeden, C., Kels, H., Hambach, U., Schulte, P., Protze, J., Eckmeier, E., Marković, S.B., Klasen, N., Lehmkuhl, F., 2016. Three climatic cycles recorded in a loess-palaeosol sequence at Semlac (Romania) – Implications for dust accumulation in south-eastern Europe. Quaternary Science Reviews 154, 130-142.

Zeeden, C., Hambach, U., Veres, D., Fitzsimmons, K., Obreht, I., Bösken, J., Lehmkuhl, F., 2018. Millennial scale climate oscillations recorded in the Lower Danube loess over the last glacial period. Palaeogeography, Palaeoclimatology, Palaeoecology 509, 164-181.

Zhao, G.Y., Liu, X.M., Chen, Q., Lü, B., Niu, H.W., Liu, Z., Li, P.Y., 2013. Paleoclimatic evolution of Holocene loess and discussion of the sensitivity of magnetic susceptibility and median diameter. Quaternary International 296, 160-167.